

EPA-600/2-77-022
January 1977

Environmental Protection Technology Series

A REAL-TIME MEASURING DEVICE FOR DENSE PARTICULATE SYSTEMS



Industrial Environmental Research Laboratory
Office of Research and Development
U.S. Environmental Protection Agency
Research Triangle Park, North Carolina 27711

RESEARCH REPORTING SERIES

Research reports of the Office of Research and Development, U.S. Environmental Protection Agency, have been grouped into five series. These five broad categories were established to facilitate further development and application of environmental technology. Elimination of traditional grouping was consciously planned to foster technology transfer and a maximum interface in related fields. The five series are:

1. Environmental Health Effects Research
2. Environmental Protection Technology
3. Ecological Research
4. Environmental Monitoring
5. Socioeconomic Environmental Studies

This report has been assigned to the ENVIRONMENTAL PROTECTION TECHNOLOGY series. This series describes research performed to develop and demonstrate instrumentation, equipment, and methodology to repair or prevent environmental degradation from point and non-point sources of pollution. This work provides the new or improved technology required for the control and treatment of pollution sources to meet environmental quality standards.

EPA REVIEW NOTICE

This report has been reviewed by the U.S. Environmental Protection Agency, and approved for publication. Approval does not signify that the contents necessarily reflect the views and policy of the Agency, nor does mention of trade names or commercial products constitute endorsement or recommendation for use.

EPA-600/2-77-022

January 1977

A REAL-TIME
MEASURING DEVICE FOR
DENSE PARTICULATE SYSTEMS

by

P.W. Chan, C.Y. She, C.W. Ho, and A. Tueton

Colorado State University
Fort Collins, Colorado 80523

Grant No. R803532-01-0
ROAP No. 21ADL-018
Program Element No. 1AB012

EPA Project Officer: William B. Kuykendal

Industrial Environmental Research Laboratory
Office of Energy, Minerals, and Industry
Research Triangle Park, NC 27711

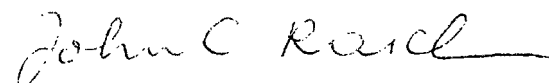
Prepared for

U.S. ENVIRONMENTAL PROTECTION AGENCY
Office of Research and Development
Washington, DC 20460

Foreword

Pollution in the atmosphere is now recognized as a serious problem. In a varying degree it affects all living things. Since man is the major polluter, he must accept his responsibility to find ways to measure and control air quality. The Physics Department of Colorado State University has, as part of its research program, projects to develop methods of monitoring the quantity and the movement of air-borne particles.

This report describes the design and the testing of a device which counts and determines the size distribution of particles in the air passing through a small volume. This is done by detecting and analyzing the light scattered by the particles. The range of particle sizes that can be measured by this method is important since it corresponds closely to the particle sizes that are retained in the lungs. In situ measurements are possible with this instrument, because the particles are not removed from the normal air flow for the measurement. In addition, the size distribution and total number of particles are obtained as an accumulation with time so the measurements are in real time.



John Raich, Chairman
Department of Physics
Colorado State University
Fort Collins, Colorado

CONTENTS

Figures	iv
Tables	vi
Acknowledgment	vii
I. Introduction, Conclusions, and Recommendations . . .	1
II. Theoretical Background	3
2-1 Mie scattering theory	3
2-2 Application to particle sizing	12
III. Instrumentation	18
3-1 General	18
3-2 The optical module	18
3-3 Electronic module	20
IV. Experimental Methods, Results and Analysis	29
4-1 Experiments using artificially generated pulses	29
4-2 Tests made on real particles	36
V. Summary and Future Work	56
References	58

FIGURES

<u>Number</u>		<u>Page</u>
2-1	Scattering diagram of plane electromagnetic wave diffracted by a sphere	6
2-2	Variation of scattered lobes with size	6
2-3	Detector output for different concentrations	6
2-4	Polar plot of Mie scattering functions for $\alpha=0.2$	7
2-5	Polar plot of Mie scattering functions for $\alpha=1.0$	8
2-6	Polar plot of Mie scattering functions for $\alpha=2.0$	9
2-7	Polar plot of Mie scattering functions for $\alpha=5.0$	10
2-8	Intensity ratio against size for wavelength = 0.6328 μm	11
2-9	Plots of $y=e^{-x^2}+e^{-(x-t)^2}$	15
2-10	Plots of $y=e^{-x^2}+0.5e^{-(x-t)^2}$	16
3-1	The optical module	19
3-2	Block diagram of processing circuit	21
3-3	Circuit diagram for particle sizing instrument	22
3-4	Input and output waveforms on comparator A-8	24
3-5	a) Timing diagram for discrete pulses	24
	b) Timing diagram for two overlapping pulses	25
	c) Timing diagram for pulses too close together	25
4-1	Typical distribution for artificial pulses of fixed ratio	30

<u>Number</u>		<u>Page</u>
4-2	Distribution for fixed ratio pulses of very low amplitude	30
4-3	Output channel number plotted against input ratio (I_{10}/I_5)	33
4-4	Output channel number plotted against input ratio (I_5/I_{10})	34
4-5	Response of processing circuit to two overlapping pulses	35
4-6	Calibration curves using methylene blue and DOP particles	39
4-7	Intensity ratio against size for different refractive indices	40
4-8	a) Distribution for methylene blue particles of diameter $2.12\mu\text{m}$	41
	b) Distribution for methylene blue particles of diameter $2.67\mu\text{m}$	41
	c) The two above distributions superimposed on each other	42
4-9	Distribution obtained using one photomultiplier . .	42
4-10	Relative response profiles for the 5° and 10° collection systems	46
4-11	Simplified optical collection system for theoretical analysis	47
4-12	Theoretical plots of relative power intercepted against displacement for different values of iris diameters	49
4-13	Typical distribution for DOP smoke of high concentration	55

TABLES

<u>Number</u>		<u>Page</u>
2-1	Probabilities of n particles in focal volume for various \bar{N}	13
4-1	Results of calibration using artificial sources . . .	32
4-2	Tabulation of I_5/I_{10} against output channel number	32
4-3	Results of calibration using the Berglund-Liu generator	37
4-4	Theoretical values of intercepted power against position	50
4-5	Experimental results for DOP smoke	52
4-6	Comparison of theoretical and experimental count rates	54

ACKNOWLEDGMENT

We wish to thank Mr. W. B. Kuykendal of the Industrial Environmental Research Laboratory, Research Triangle Park, for many helpful discussions and Mr. J. Abbott for lending us the Berglund-Liu aerosol generator for use in this project.

Chapter I

INTRODUCTION, CONCLUSIONS, AND RECOMMENDATIONS

Recent concern over the quality of the environment has raised interest in the field of particle sizing. Particles with diameters below several microns are of most interest because they can remain suspended in air for a long time and can be deposited in human lungs. However, for this range of sizes a successful technique for measuring the particle size distribution in real time over a wide range of concentrations has yet to be developed. At present, the methods for determining particle size distributions can be classified into two categories.¹ The first class includes non-optical methods such as electron microscopy or passing the sample through a series of stages in an impactor and then weighing them successively. These methods involve significant perturbation of the particles under investigation. In this process the particle size distribution may be altered. Besides, samples have to be taken and process time is slow.

Methods of the second category utilize light sources and can be described as optical methods. The optical methods are based on the fact that a particle cloud provides inhomogeneities in the medium and would therefore scatter light. Different size particles have different light scattering properties. Thus, by illuminating the particle cloud with a light source and then observing the transmission, extinction or scattering of the source, some information about the particle sizes can be obtained. In the transmission method a light source illuminates the particle cloud and the resultant transmission is determined as a function of wavelength. Using this data it is possible to extract some information about the size distribution of the cloud.² In the photometric light scattering method, light scattered simultaneously from a large number of particles in part of the incident beam is collected and analyzed. Although they introduce no perturbation to the system under investigation, these methods have accuracy very much dependent on the particular size distribution it is measuring. Besides, quite complicated procedures are involved to obtain the desired results from experimental data. Usually these have to be performed on a digital computer. Thus, these methods do not provide real time, *in situ* monitoring of particle size distributions.

The single particle counter looks at one particle at a time by making its sensitive focal volume very small. The light scattered by a particle at a certain angle (or over a range of angles) is collected.³ From the pulse height distribution of the resultant signal the particle

size distribution can be determined. Because the light scattered from a particle depends not only on its size but also its refractive index, this technique cannot handle polydispersed systems with unknown (and often complex) indices of refraction. Due to the fact that this situation is often encountered in actual practice, better techniques need to be developed.

Hodkinson⁴ made an important contribution when he realized that the shape of the forward lobe scattered from a particle is due primarily to Fraunhofer diffraction and has therefore a minimum dependence on refractive index. Thus, by measuring the intensity ratio of scattered light at two forward angles, the particle size can be determined quite independent of refractive index. This instantaneous intensity ratio technique provides a means of monitoring polydispersed systems in real time. However, because the particles have to be viewed one at a time, the concentration that can be handled by this technique is quite low. It is limited by the smallest focal region that can be achieved in practice.

This report deals with the design, building and testing of an instrument that is capable of handling dense particulate systems. Chapter II gives the fundamental Mie scattering theory and intensity ratio technique that form the background for this research. The concepts for increasing the concentration handling capability are also discussed. With those concepts in mind, the optical and electronic instrumentation are designed. Chapter III describes the instrumentation in detail and explains how the proposed instrument applies the theoretical concepts. In Chapter IV the performance of this instrument is discussed. Its limitations are evaluated and the maximum concentration that can be handled is investigated. Finally, in Chapter V the results obtained from this study are summarized. Suggestions for improving the instrument are made and possible future work in this area is suggested.

A real-time device having the potential of increasing the particulate concentration handling capability by one order of magnitude has been constructed and tested. It is based on analyzing the intensity ratio of scattered light at two angles. Contrasted to present particle sizing devices the device allows more than one particle to be viewed in the focal volume at any instant and selects the scattered light pulses randomly for data processing. The device can handle an average of $\bar{N} = 2.5$ particles in the focal volume (compared to $\bar{N} = 0.2$ of other similar devices) for particle size from 0.6 to 3.5 μm in real-time with good accuracy and resolution.

Immediate improvement on the optical module to increase the concentration handling capability by one order of magnitude to 10^7 particles per c.c. is of utmost importance. The system's resolution should be improved and the size range handling capability should be enlarged to both smaller and larger particles. A rugged device could then be built for field testing and use.

Chapter II

THEORETICAL BACKGROUND

The discussion below is based on spherical particles. For non-spherical particles, which are often encountered in actual practice, theoretical solutions have been solved only for certain particular cases (e.g., cylinders, ellipsoids). It is, however, noticed that a poly-dispersed, randomly oriented nonspherical system of particles has the same gross light scattering characteristics as that for spherical particles if the scattering angles are in the forward direction.⁵ Hence the results below are applicable generally.

2-1 Mie Scattering Theory

The problem of scattering of a plane monochromatic electromagnetic wave by a sphere of arbitrary size and refractive index has been solved by Mie in 1908.⁶ In short, this is a problem of solving Maxwell's Equations with the appropriate boundary conditions imposed by the presence of the sphere in the field.

Consider a plane wave travelling along the positive z axis and incident on the sphere as shown in Figure 2-1.

Here the origin is taken at the center of the sphere, the positive z axis along the direction of incident wave propagation and the polarization of the wave is in the direction of the x axis. The incident field has unit amplitude for simplicity.

In spherical coordinates, the resultant wave equation is variable separable. The scattered components of the electric field E_θ and E_ϕ are spherical outgoing waves given by:

$$E_\theta = \frac{i}{kr} e^{-ikr+i\omega t} \cos \phi S_2(\theta, \alpha, m)$$
$$-E_\phi = \frac{i}{kr} e^{-ikr+i\omega t} \sin \phi S_1(\theta, \alpha, m)$$

where r is the distance from the origin to point of observation

$$\alpha = \text{size parameter} = \frac{\pi d}{\lambda}$$

m = refractive index of sphere relative to the medium

d = diameter of sphere

k = wave number = $\frac{2\pi}{\lambda}$

S_1, S_2 are scattering functions, each being a sum of infinite series of Legendre Polynomials and spherical Bessel functions.

The radial component E_r may also be derived from Mie's solution but it tends to zero with a higher power of $1/r$.

In general, the scattered light is elliptically polarized even in this case, when the incident radiation is linearly polarized. This is because the functions S_1 and S_2 are complex numbers with different phases.

The intensity at the point of observation can thus be calculated.

$$\begin{aligned} I &= I_\theta + I_\phi \\ &= |E_\theta|^2 + |E_\phi|^2 \\ &= \frac{1}{k^2 r^2} \cos^2 \phi |S_2(\alpha, m, \theta)|^2 + \frac{1}{k^2 r^2} \sin^2 \phi |S_1(\alpha, m, \phi)|^2. \end{aligned}$$

Putting

$$\begin{aligned} |S_1(\alpha, m, \phi)|^2 &= i_1(\alpha, m, \theta); \quad |S_2(\alpha, m, \theta)|^2 = i_2(\alpha, m, \theta) \\ k &= \frac{2\pi}{\lambda}. \end{aligned}$$

The equation becomes

$$I = \frac{\lambda^2}{4\pi^2 r^2} [\sin^2 \phi i_1(\alpha, m, \theta) + \cos^2 \phi i_2(\alpha, m, \theta)]$$

For an incident wave of intensity I_0 ,

$$I = \frac{\lambda^2 I_0}{4\pi^2 r^2} [\sin^2 \phi i_1(\alpha, m, \theta) + \cos^2 \phi i_2(\alpha, m, \theta)] \quad (2-1)$$

Equation 2-1 gives the expression for linearly polarized incident light of intensity I_0 . If the incident light is randomly polarized, as in the case of natural light, an averaging over the angle ϕ has to be performed to get the intensity scattered. Since $\overline{\cos^2 \phi} = \overline{\sin^2 \phi} = 1/2$, the expression for scattered intensity becomes:

$$I = \frac{\lambda^2 I_0}{8\pi r^2} [i_1(\alpha, m, \theta) + i_2(\alpha, m, \theta)] \quad (2-2)$$

Simplified theoretical solutions exist for various classes of particle sizes and refractive index.⁷ For example, for small particles ($\alpha \ll 1$, $|m| \ll 1$), the first term in the expressions for i_1 and i_2 is predominant and scattering is due primarily to electric dipole oscillations. For large particles (an order of magnitude greater than the wavelength), the scattering pattern can be found by superposition of Fraunhofer diffraction and reflection and refraction. For refractive index close to 1, the Rayleigh-Gans theory may be applied to give a simpler solution. However, for the particle size range of interest (0.05 - 10 μm), no simplifications exist and the full Mie solution must be used.

From equations 2-1 and 2-2 one can observe that the scattered intensity does depend on the size parameter α . Better physical insight and ways to utilize the Mie scattering theory for practical applications is not easy to achieve because of the complexity of the functions i_1 and i_2 . Fortunately, during the past decade many numerical tabulations of the scattering functions (i_1 and i_2)^{8,9} for spheres with different sizes and refractive indices are available. With the help of these tables, full potential of using the Mie theory in practical applications can be appreciated. Figure 2-2 shows qualitatively the variations of scattering pattern with size.

It is observed that, for small particles, the forward lobe is wide with a small backward lobe. As the particle size is increased, the forward scattering lobe narrows and becomes strongly enhanced, the backward scattering lobe becomes somewhat enhanced, and a number of weak side lobes develop. The number of side lobes increases with increasing particle size. Hence, by detecting the intensity variation scattered from the forward lobe, information about the size of the particle can be obtained. Figures 2-4 to 2-7 show polar plots of the two components of intensity as a function of scattering angle (0 - 90°) for different sizes and refractive indices. From these figures, one notices that the scattered intensity also depends strongly on the refractive index. Therefore, to size a polydispersed system of particles with unknown index of refraction, the scattered intensity at one angle does not give sufficient data. However, one important observation is that the shape of the forward lobe is by and large independent of refractive index and varies only with particle size. Hodkinson noticed this and proposed that, by measuring the intensity scattered at two different forward angles and then taking a ratio of the two, the effect of refractive index can be minimized. To illustrate the variation of intensity ratio with size, curves of intensity ratio vs. size within the forward lobe are reproduced in Figure 2-8. This figure is reproduced after Kreikebaum and Shofner¹⁰ and is calculated assuming spherical particles with imaginary component of refractive index > 1 . Depending on the range of particle sizes to be covered, a pair of angles can be selected. The 10°/5° is used as an example for discussion. From this figure several characteristics of this technique can be observed:

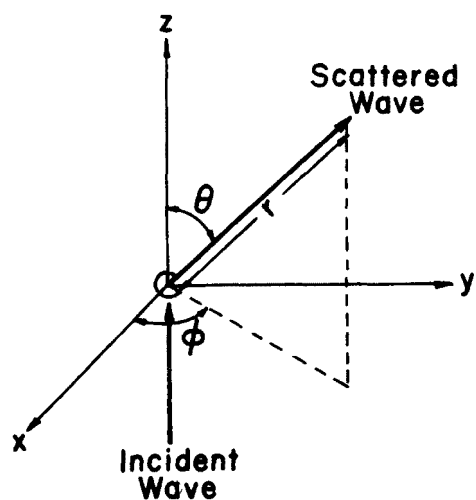


Figure 2-1. Scattering diagram of plane electromagnetic wave diffracted by a sphere.

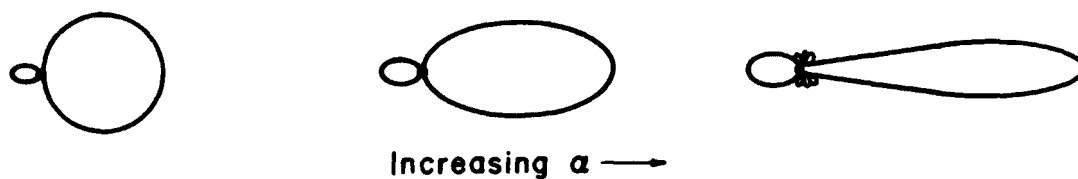


Figure 2-2. Variation of scattered lobes with size ($\alpha = \pi d/\lambda$).

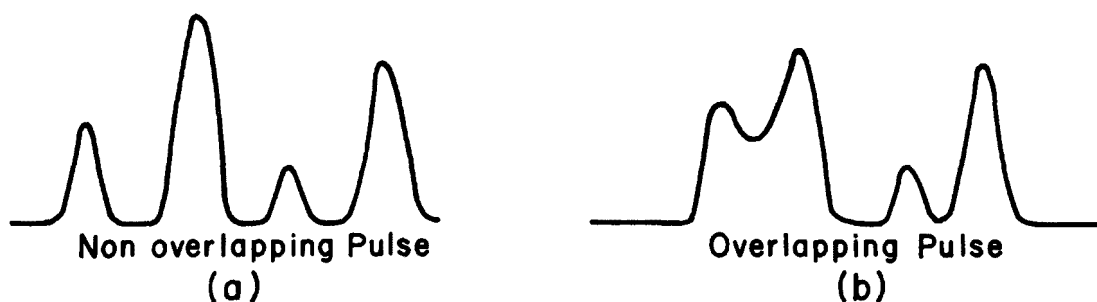


Figure 2-3. Detector output for different concentrations:

a) Low concentrations

b) Higher concentrations

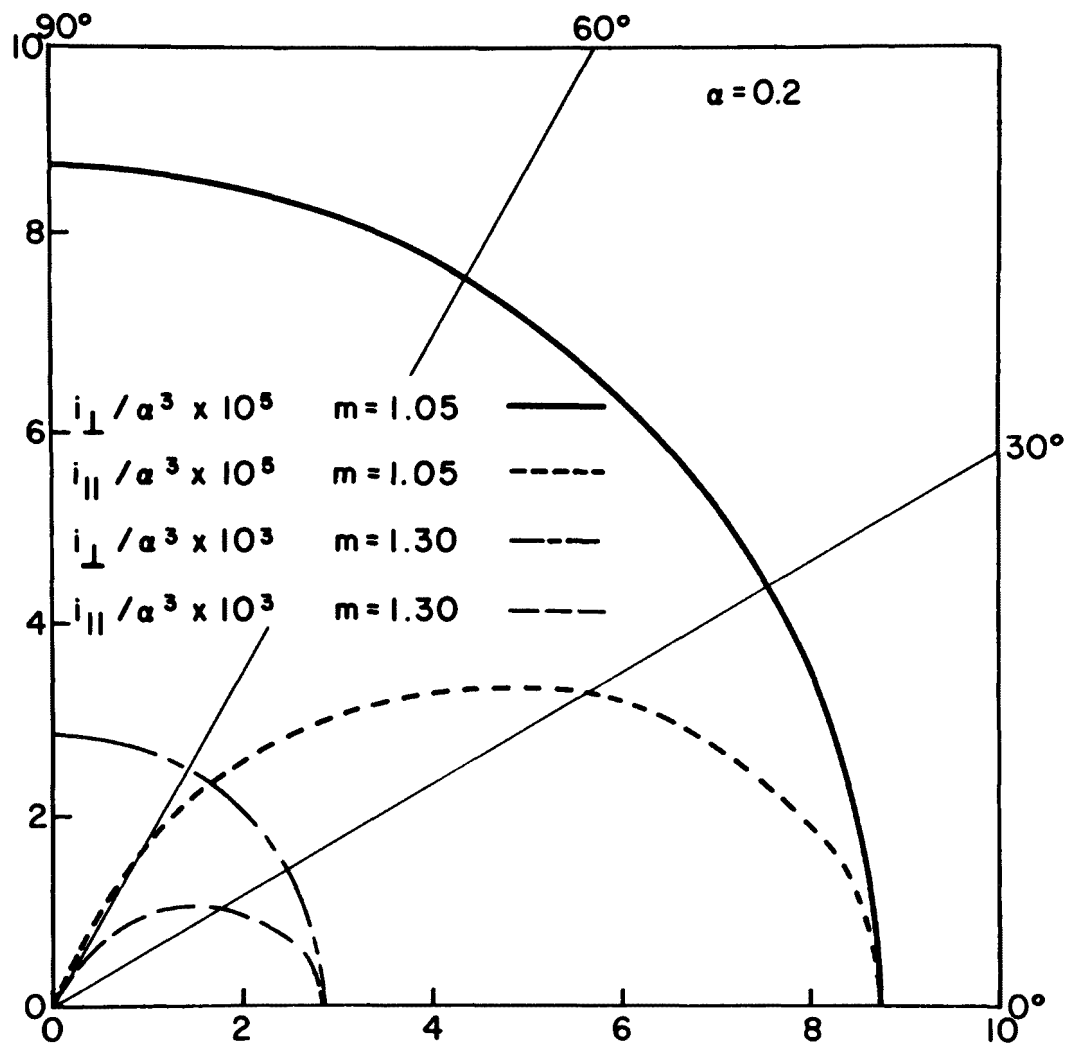


Figure 2-4. Polar plots of Mie scattering functions for size parameter $\alpha = \pi d / \lambda = 0.2$ of different polarization and refractive index.

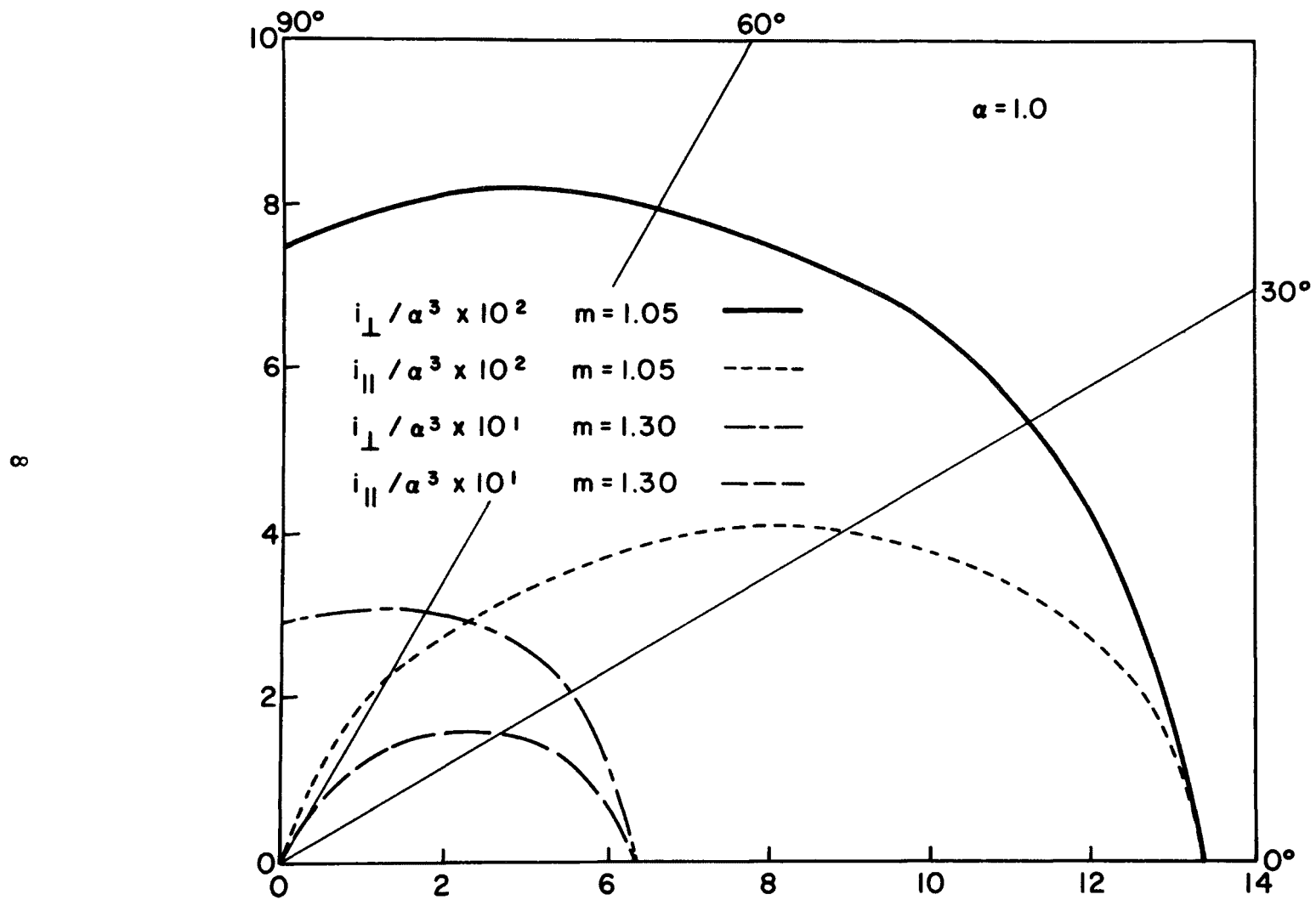


Figure 2-5. Polar plots $\alpha = \pi d / \lambda = 1.0$.

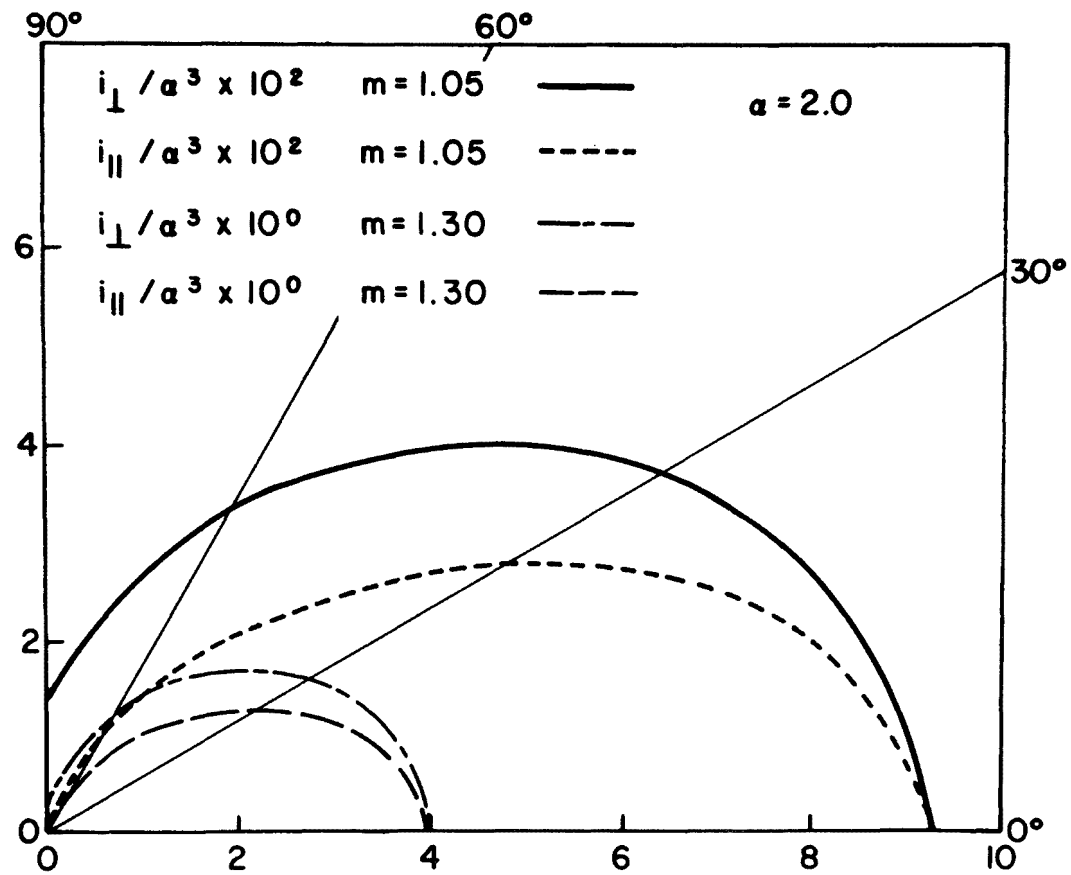


Figure 2-6. Polar plots $\alpha = \pi d / \lambda = 2.0$.

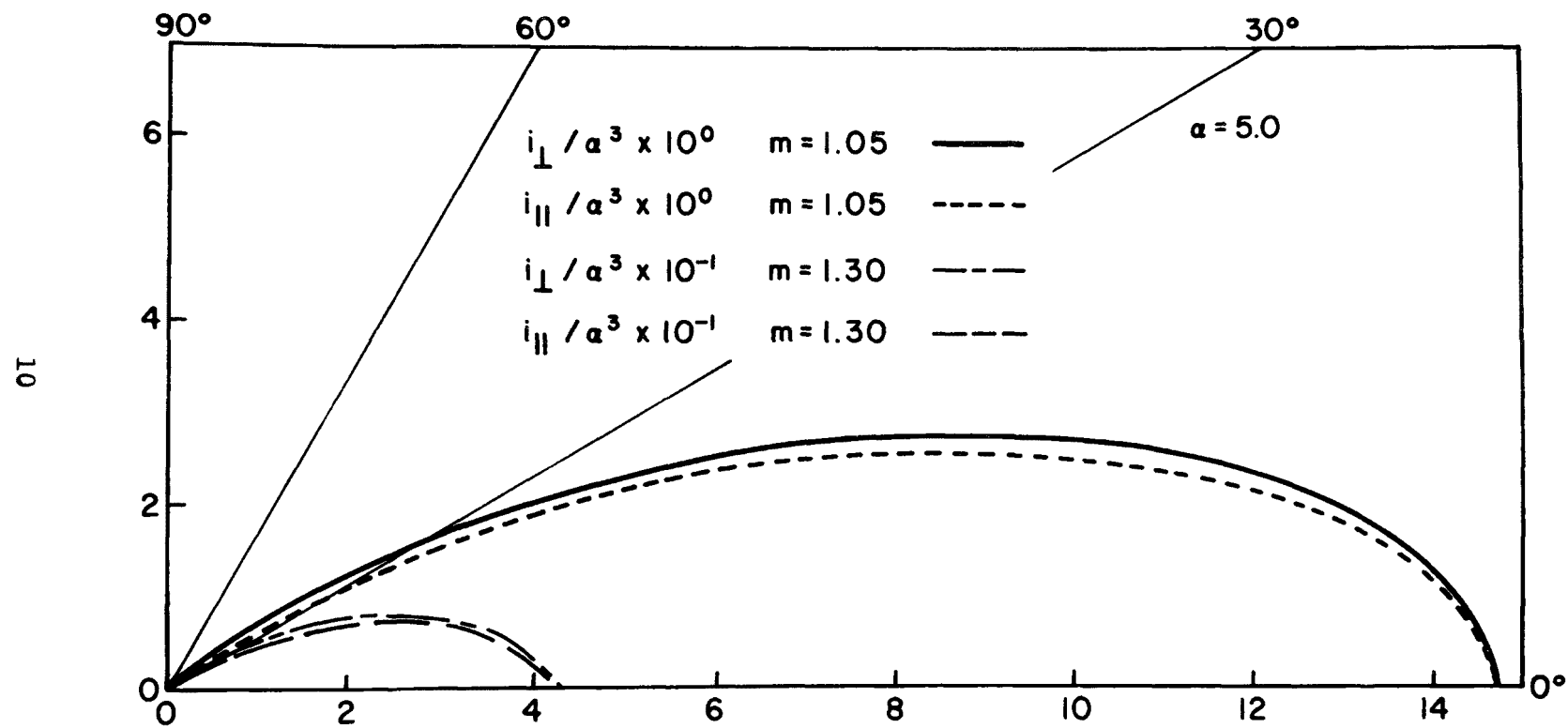


Figure 2-7. Polar plots $\alpha = \pi d / \lambda = 5.0$.

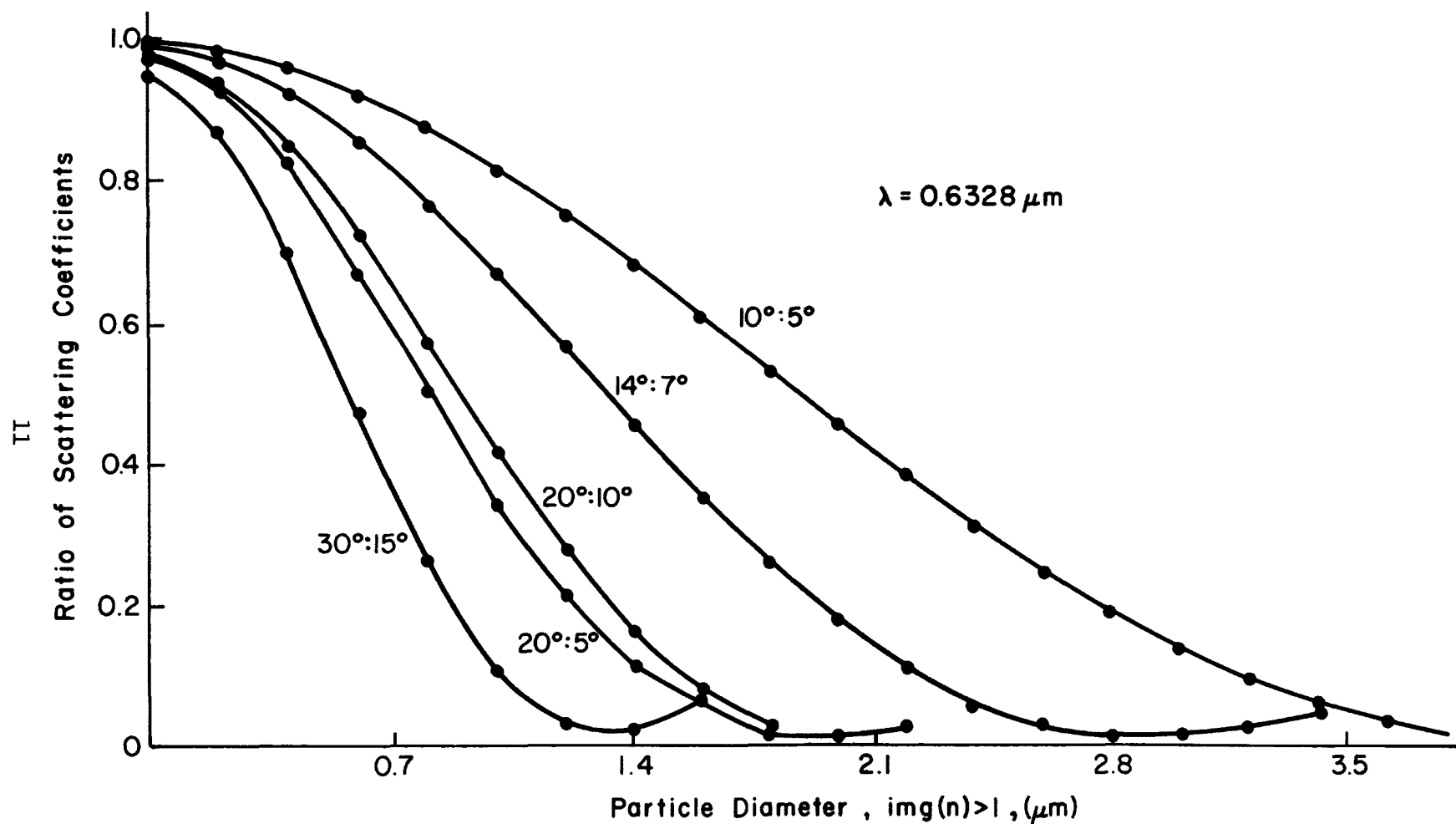


Figure 2-8. Intensity ratio vs. size for wavelength = 0.6328 μm .

1) The curve is decreasing with increasing particle size inside the forward lobe. Hence a one to one relationship between particle size and intensity ratio is obtained.

2) The curve is relatively flat for small α , i.e., the intensity ratio is insensitive to particle size variations. This imposes a limit on the smallest size that can be measured.

3) When the particle size becomes large, the scattered intensity at the outer angle (10° in this case) becomes smaller because it is approaching its first minimum. The upper limit to particle sizing is thus set by the sensitivity of the scattered intensity detector and its background noise level. To extend the upper limit to a larger size, a smaller pair of angles may be used (e.g., $2.5^\circ/5^\circ$). For the $10^\circ/5^\circ$ case, using a visible light source, the practical range of size detection is $\sim 0.1\text{--}4\mu\text{m}$.

4) Figure 2-8 is plotted using an imaginary component of index > 1 . Particles with large absorption actually give a smoother intensity ratio $-\alpha$ curve. For real indices, small oscillations can be observed in the curve (Figure 4.7) and can cause errors. In any case the maximum error due to refractive index is estimated to be 15-20 percent.

2-2 Application to Particle Sizing

Two techniques applying this principle may be used for measuring particle size. They are described below:

1) Time averaged measurements: If two slow detectors are used to detect the scattered intensity from a cloud of particles, a time-average will be measured. The resultant intensity ratio will be given by the following formula:

$$\rho(\theta_1/\theta_2) = \frac{\int i(\theta_1) f(\alpha) d\alpha}{\int i(\theta_2) f(\alpha) d\alpha}$$

where $f(\alpha)$ represents the particle size distribution function.

Theoretical calculations of $\rho(\theta_1/\theta_2)$ for various bell-shaped distributions with mean $\bar{\alpha}$ and deviation ρ can be made. By comparing the measured results with those calculated, the parameters of the size distribution ($\bar{\alpha}$ and ρ) can be deduced. This method is, however, time consuming. Furthermore, only certain distributions can be handled and it cannot be considered as a real-time method to monitor size distributions. Hence this topic will not be discussed further.

2) Instantaneous measurements: The advantages of intensity ratio method can be fully utilized if the particles can somehow be viewed one at a time and the intensity ratio measured and recorded. The scheme is as follows:

A light source (laser for example) is focused down to a very small volume and the particle cloud under investigation is allowed to flow through the focal volume. When there is no particle flowing through the focal volume at a particular instant, the detectors for the two angles give no signal other than background noise fluctuations. Whenever a particle passes through the focal volume, light is scattered to yield outputs on the two detectors. The pulses are immediately processed and the ratio of the intensities taken. By means of a pulse height analyzer, the frequency of occurrence of intensity ratio current pulses as a function of pulse height (and hence particle size) can be obtained. If the pulse height analyzer is calibrated beforehand in terms of particle size, the distribution can be obtained immediately. By taking a ratio of the scattered intensities, experimental errors due to variations in source output power can be eliminated. The fact that this technique does not assume anything about the shape of particle size distribution means that it can handle nearly any type of particle distributions. The desirability of the method over method (1) is thus evident.

One flaw in this technique is that only one particle at a time is allowed in the focal volume. This would set an upper limit on the concentration that can be correctly detected. Consider a unit focal volume through which a particle system of average concentration \bar{N} /unit volume is flowing. Assuming that the particles are distributed randomly in space at a particular instant, the probability of n particles present in the unit volume at any given instant is given by the Poission distribution

$$P(n) = \frac{e^{-\bar{N}} \bar{N}^n}{n!} \quad (2-3)$$

The following table gives some values of probability for different values of average concentration \bar{N} :

Table 2-1. Probabilities of n particles in focal volume for various \bar{N} .

\bar{N}	P(0)	P(1)	P(2)	P(3)
1	3.68×10^{-1}	3.68×10^{-1}	1.84×10^{-1}	6.13×10^{-2}
0.8	4.49×10^{-1}	3.59×10^{-1}	1.44×10^{-1}	3.83×10^{-2}
0.6	5.49×10^{-1}	3.29×10^{-1}	9.88×10^{-2}	1.98×10^{-2}
0.3	7.41×10^{-1}	2.22×10^{-1}	3.33×10^{-2}	3.33×10^{-3}
0.2	8.19×10^{-1}	1.64×10^{-1}	1.64×10^{-2}	1.09×10^{-3}
0.1	9.05×10^{-1}	9.05×10^{-2}	4.52×10^{-3}	1.51×10^{-4}

The above figures indicate that in order to keep the probability of more than one particle in the volume at a given instant quite low, the average concentration that can be handled for a unit volume is much less than 1. For example, for an error of ~ 1.64 % maximum, maximum \bar{N} that can be handled is 0.2 (in which case $P(2) = 0.0164$). For a volume as small as 10^{-7} cm^3 , which can be achieved by using a laser as light

source and good focusing lens, the maximum concentration detectable is about $2 \times 10^6/\text{cm}^3$. Dense particle systems have to be diluted before being counted; and in the dilution process the size distribution may be altered.

It is realized that by committing oneself to just one particle in the focal volume at a time, the measuring system is not very efficient¹¹. Larger concentrations can be handled if the number of scatterers in the volume is greater than unity.

When there is just one particle traversing the focal volume at a particular instant, the detector outputs record non-overlapping pulses as shown in Figure 2-3a.

If there is more than one particle in the scattering volume, the detector outputs will record overlapping pulses like one shown in Figure 2-3b. In this case one assumes that the particles enter the focal volume at slightly different instants so that two peaks can be observed. The intensities are also assumed to add. If one can somehow identify the two pulses and process them independently, an improvement in the detectable concentration can be achieved. Referring to Table 2-1, if two overlapping pulses can be identified, the maximum concentration is $\bar{N} \sim 0.6$ (in which case $P(3) = 1.98 \times 10^{-2}$) for the same degree of accuracy. In principle, if more overlapping pulses can be handled, the manageable concentration is increased even more. However, there is a rigid limit to this and the case is discussed below.

Consider a TEM₀₀ beam as light source. The intensity distribution at the cross section⁰⁰ is then Gaussian. Therefore the scattered light pulses will also be Gaussian. In Figures 2-9 and 2-10, some theoretical curves for two Gaussians with different degrees of overlap are shown. In Figure 2-9, the two pulses are of same peak amplitude, while in Figure 2-10, one amplitude is half the other.

It is seen that as the two pulses come closer to each other, the dip in the middle becomes less and less. Then, at some degree of overlap dependent on their relative amplitude, the two pulses merge into a bigger pulse (Figure 2-9a and 2-10a). Experimentally the above case cannot be resolved and erroneous results will be obtained. Besides, when the concentration is too high, the pulses tend to become small ripples riding on a d.c. level and their intensity ratios do not necessarily represent the particle size.

One way of solving the above problem is to place a limit on the degree of overlap the measuring system will process. If one can, by proper instrumentation, arrange the data processing system such that pulses too close together are discarded, the error due to the above effect can be minimized. In doing this one assumes that the inter-arrival time of particles is random and independent of its size. In other words, two big particles have the same probability of arriving at the focal volume at nearly the same time as that of two small particles. Thus the measuring system would be sampling randomly a

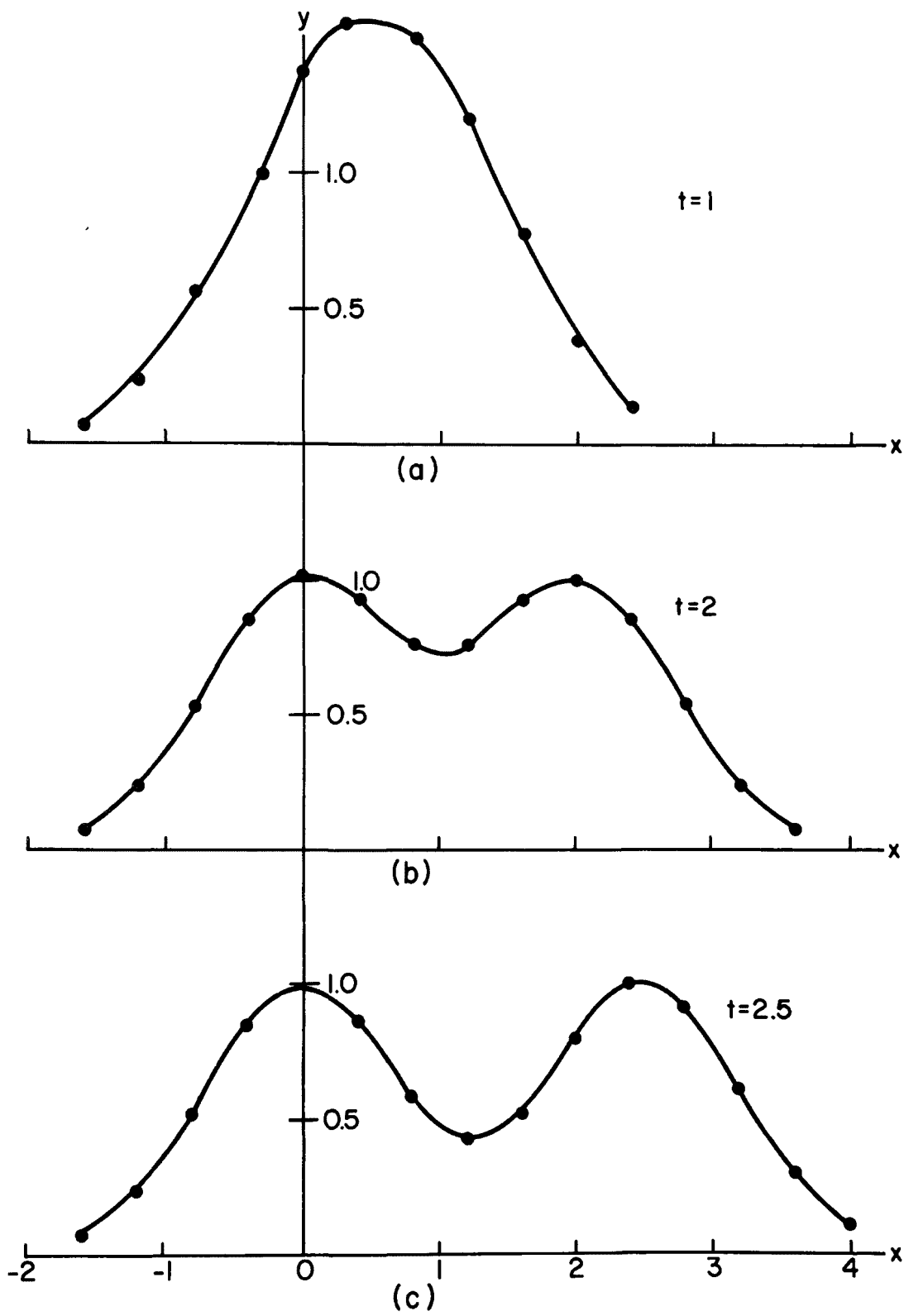


Figure 2-9. Plots of $y = e^{-x^2} + e^{-(x-t)^2}$.

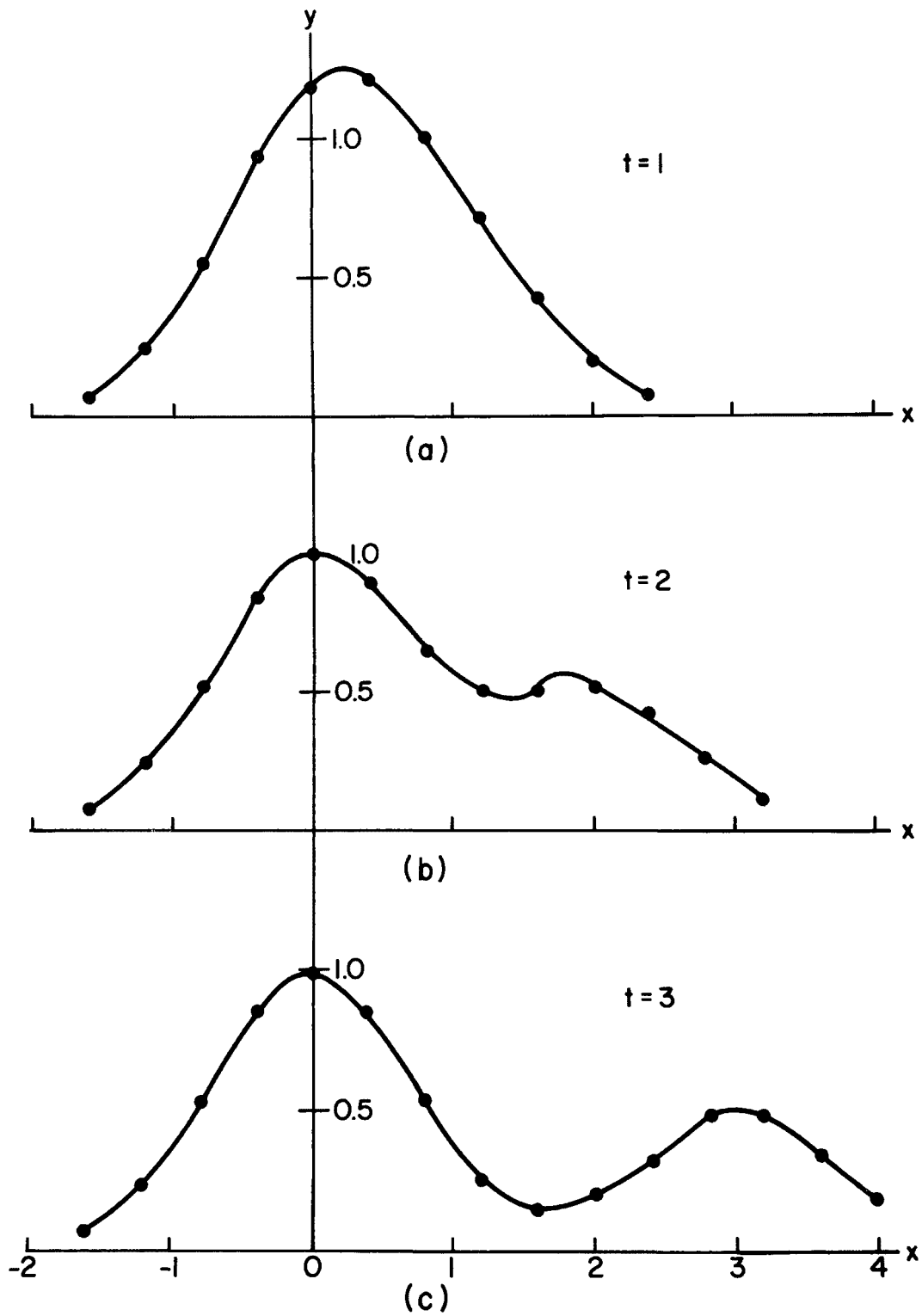


Figure 2-10. Plots of $y = e^{-x^2} + 0.5e^{-(x-t)^2}$.

distribution of particles. By the theory of statistics, the samples taken should have the same size distribution as that of the main stream.

Bearing these concepts in mind, the design of the optical and electronic system to achieve the above objectives is discussed in the next chapter.

Chapter III

INSTRUMENTATION

3-1 General

The optical system for this instrument is required to achieve the following:

- a) Define a finite sampling volume through which the system of particles under investigation traverses.
- b) Collect the light scattered from those particles at two forward angles, 5° and 10° in this case.

Main design considerations are the minimization of stray light and the minimization of focal volume. The first one determines the signal to noise ratio of the instrument, while the second one determine the maximum concentration the system can handle.

The electronic module does the processing of the light pulses collected. It is required to take the ratio of the peak value of the pulses scattered at the two angles and accumulate those values to yield the appropriate size distribution. These two modules are discussed in more detail in the following sections.

3-2 The Optical Module

Figure 3-1 shows the optical setup for this instrument. A He-Ne laser ($\lambda=0.6328\mu$) is focused down by a lens (L_1). The pinhole P is made out of flat black paper and it serves to restrict and clean up the edges of the laser beam and also reduce reflections from the lens L_2 . The light scattered at the correct angles (5° and 10°) is selected by concentric rings of appropriate diameter. The use of three of these ensures that stray light coming in at an unwanted angle is blocked out. At the other side of the rings convex lenses L_2 and L_3 are used to focus the scattered light to one point to be picked up by optical fibres. In the original arrangement, the collection slits for the 5° and 10° scattering angles were parallel. However, measurements of the focal volume revealed that the region seen by the 5° collection system did not exactly coincide with the region seen by the 10° collection system. This is due largely to spherical aberration of the lenses used. The origin of the fault is that for an uncompensated lens, parallel light that comes in near the edge of the lens has a shorter focal length

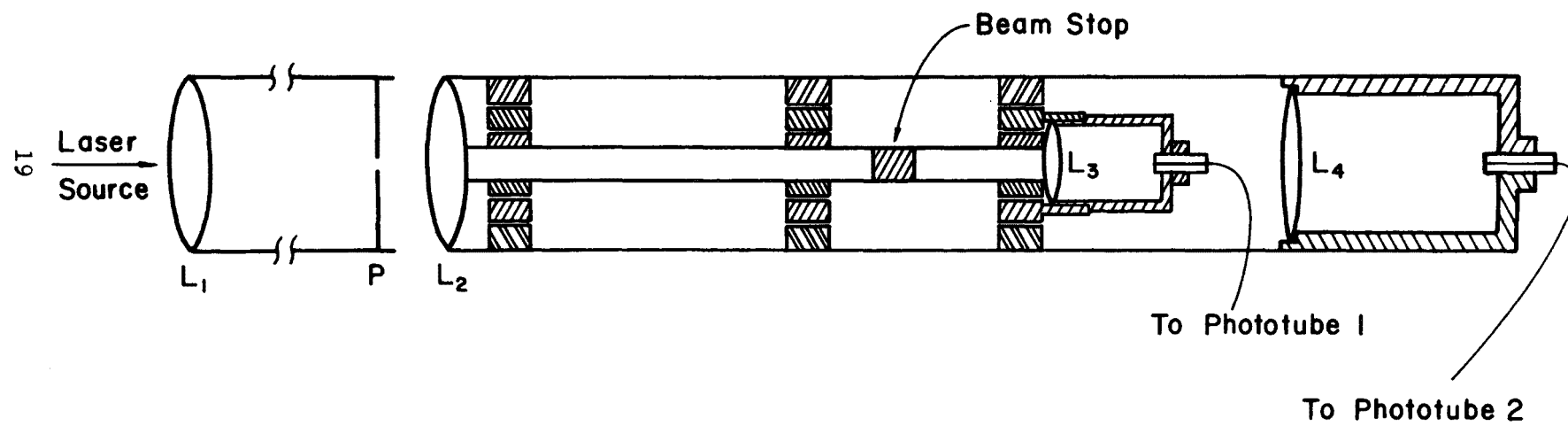


Figure 3-1. The optical module.

than light that comes in closer to the axis. If parallel light were collected for both angles, the 5° would see a region which is further away from the lens than the 10°. To correct for this, the slits for the 10° collection are made such that they collect light which is slightly converging. The inner rings (5°) collect light that comes in essentially parallel. By this method good overlap of the two focal regions can be achieved.

The entire collection system is housed in an aluminum tube. This makes the system rigid and easy to align. Stray light is also minimized to the extent that the system can operate in ambient light conditions without stray noise becoming too excessive. Its operation can be improved if appropriate spike filters are inserted in front of the collection lens to allow only light of the correct wavelength (wavelength of laser used) to pass through.

3-3 Electronic Module

The electronic module processes the photomultiplier outputs and converts them to a particular size distribution. It is designed to achieve the following objectives:

- 1) Detecting the peak value of the scattered pulses and taking the value of their ratio. This minimizes the error in the ratio due to stray background noise.
- 2) To identify two overlapping pulses due to two particles traversing the focal volume at slightly different instants and obtain their intensity ratio.
- 3) To neglect pulses that are so close to each other that the value of their ratio is no longer correctly related to their size.

Figure 3-2 shows a block diagram of the electronic processing circuit and Figure 3-3 shows a complete circuit diagram. The operation of the circuit is as follows:

The current pulses from the two photomultipliers, each terminated in 10kΩ resistors, are fed into operational amplifiers A1 and A2, which are voltage followers acting essentially as current to voltage converters. The outputs from A1 and A2 go to two sample and hold modules (Analog Devices AD583) for data processing. These voltage pulses are also fed into the timing and control unit which generates the appropriate control and coincidence signals for accurate data acquisition. Amplifiers A3 and A4 serve as isolation amplifiers for the triggering and incoming circuits. The output of A3 goes into the peak detector trigger circuit. This consists of amplifiers A5, A6 and comparator A8. Amplifier A5 is connected as an ordinary voltage inverter. A6 has a parallel R-C combination connected in its input. This has two effects: it attenuates the incoming signal a little and also tends to delay it by a small amount. However, this amplifier has a slightly bigger gain so that the output is an inverted and also

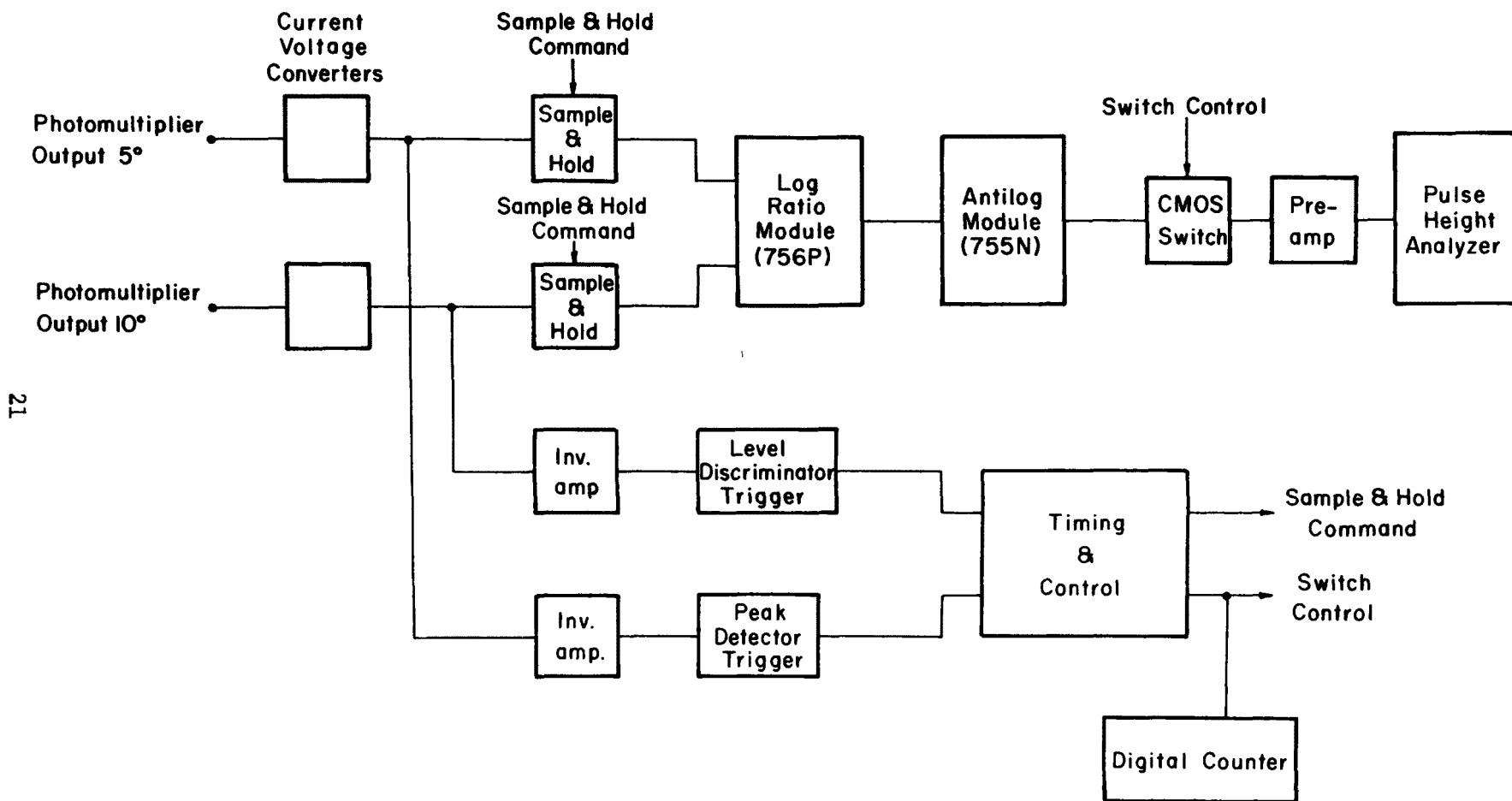


Figure 3-2. Block diagram of processing circuit.

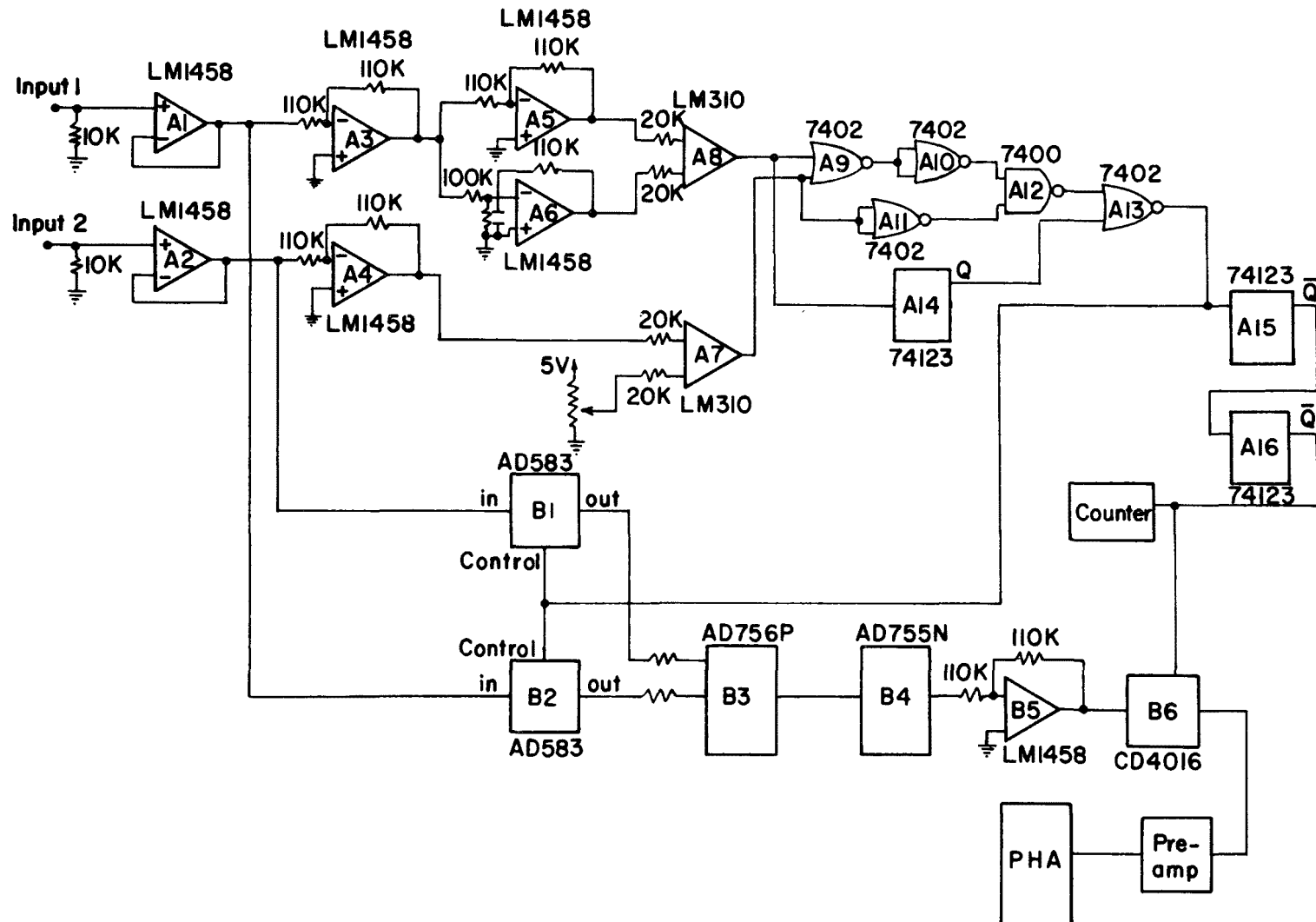


Figure 3-3. Circuit diagram for particle sizing instrument.

slightly delayed version of the input signal. This pulse and the output from A5 form the input of comparator A8. This comparator detects the crossover points and would therefore trigger whenever there is a change of slope. This is shown in Figure 3-4.

By this method the peak of the pulses can be detected with good accuracy. The amount of delay depends on the rise time of the input pulse. Hence the actual trigger point will also vary a little as the overall pulse width is varied. However, this arrangement works fine for a large range of pulse widths that are of interest.

The output of amplifier A4 is connected to comparator A7. The other input is connected to an adjustable d.c. This comparator triggers whenever the input is above the preset d.c. level. The function of this is to provide a discrimination level. Input pulses which are below this d.c. level are neglected by the system. Normally this d.c. level is set so that it is bigger than random photomultiplier fluctuations but smaller than the smallest pulse that originates from light scattered by particles in the sensitive volume.

The outputs from the two comparators (TTL level) form the basic signals for timing of the system. Figure 3-5 shows timing diagrams for the circuit. Three cases are to be considered: 1) nonoverlapping pulses, b) two overlapping pulses, and c) a series of overlapping pulses so close together that the values of their ratio no longer give a fair representation of their sizes.

First of all consider case a). The relative timing is shown in Figure 3-5a. When there is no input at all the outputs of both A7 and A8 are high. The output of A13 is therefore low. This output provides the control signal for the two sample and hold modules B1 and B2 and causes them to stay in the hold mode. When a pulse is detected comparator A7 triggers first and goes low. The output of A11 goes high. On the other hand, the output of A10 is still clamped high because peak triggering has not yet occurred. The sample and hold modules switch to the sample mode. The outputs of B1 and B2 then follow the values of the input. When the input pulse reaches its peak, comparator A8 triggers and goes low. This forces the output of A10 low and hence output of A12 high. The sample and hold control signal goes low and switches the system to hold mode, holding the peak values of the input pulses. The outputs of B1 and B2 are connected to a logarithmic module (AD756P). This module takes a ratio of the two inputs according to the following transfer function

$$e_o = -k \log \frac{i_1}{i_2} \quad (3-1)$$

where i_1 = signal current
 i_2 = 10° output in this case

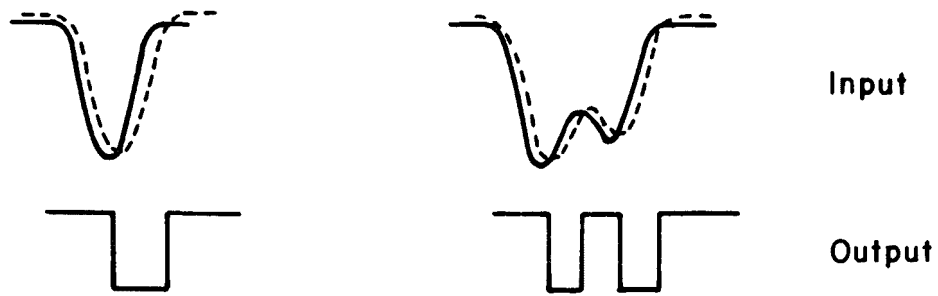


Figure 3-4. Input and output waveforms on A8.

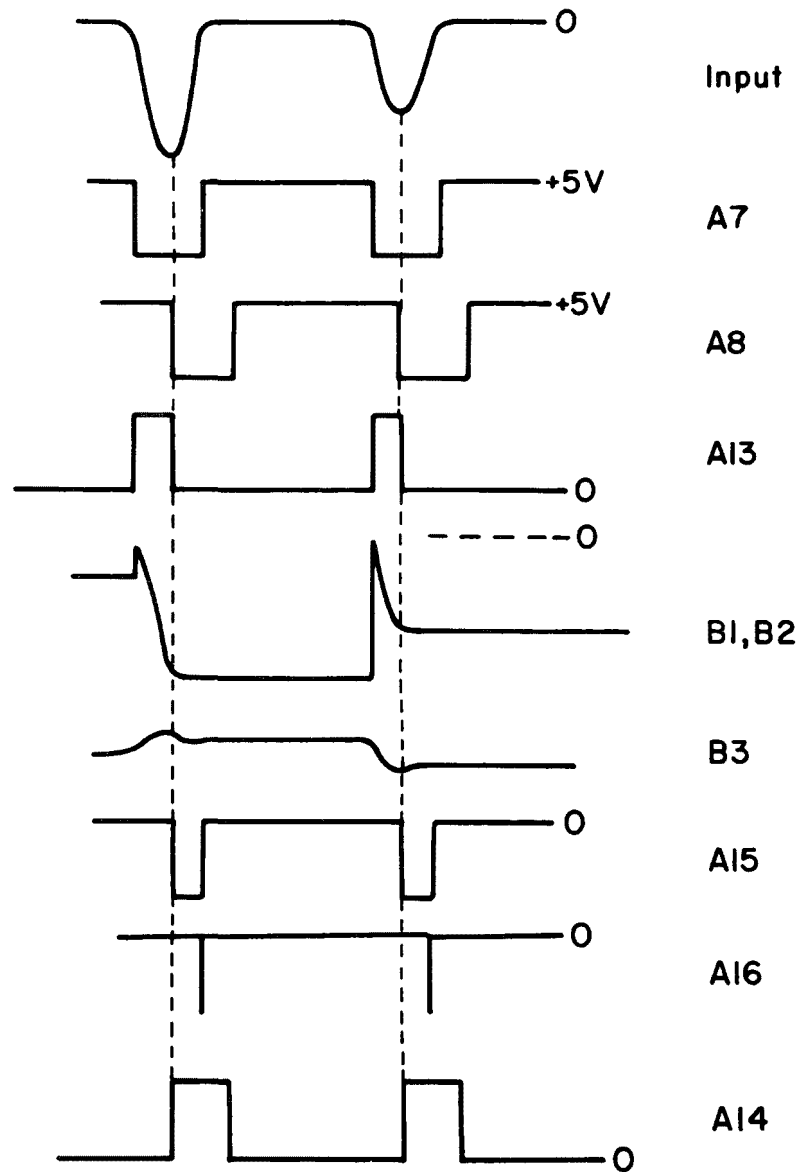


Figure 3-5a. Timing diagram for discrete pulses.

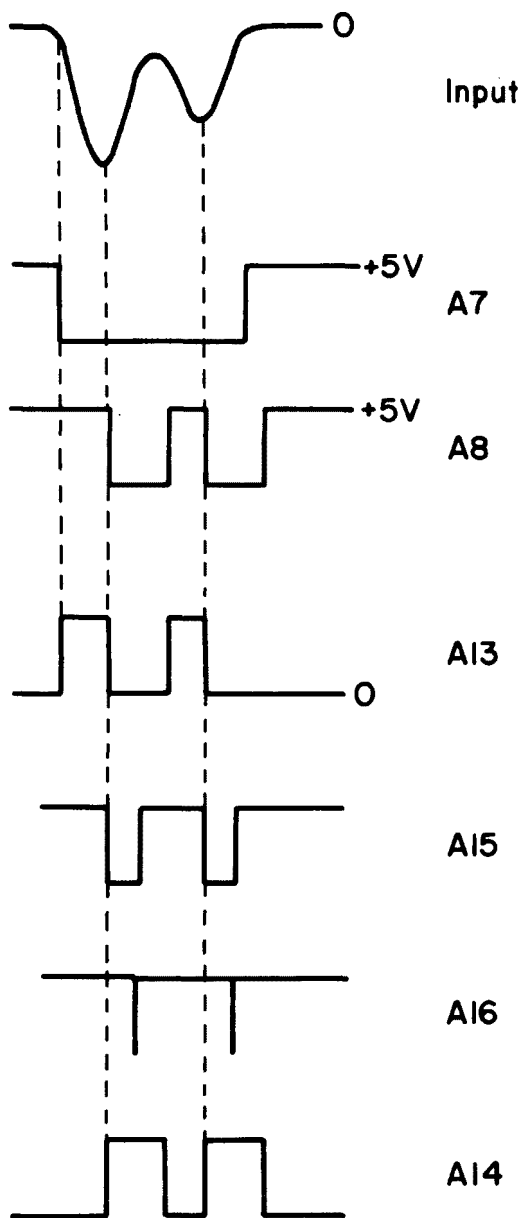


Figure 3-5b. Timing diagram for two overlapping pulses.

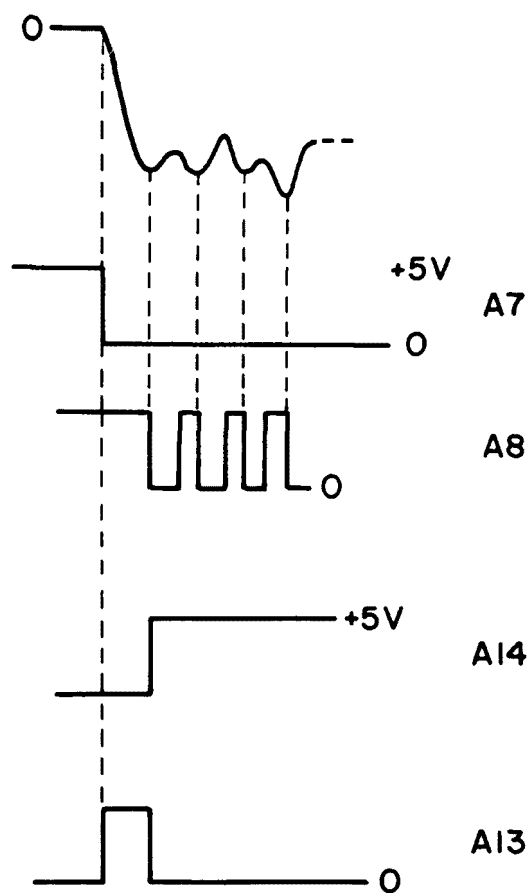


Figure 3-5c. Timing diagram for pulses too close together.

$$\begin{aligned}
i_2 &= \text{reference current} \\
&= 5^\circ \text{ output in this case} \\
k &= -1 .
\end{aligned}$$

This is followed by an antilog module with transfer equation

$$e'_o = E_{\text{ref}} 10^{-e_{\text{in}}/k} \quad (3-2)$$

where E_{ref} = reference voltage

$$= 0.1V$$

e_{in} = input voltage

$$k = 1 .$$

The overall transfer equation of the two modules is given by

$$e'_o = 0.1 \frac{i_2}{i_1} \quad (3-3)$$

There are several advantages in using a logarithmic setup. Firstly, it allows a large range of input current values. Secondly, a ratio range of a million to one can be handled. Although in the present system the antilog module is used to give a linear output, slight modifications can be made to give a logarithmic output ratio and therefore a logarithmic distribution on the pulse height analyzer. One disadvantage of these modules is that they have a relatively slow frequency response. The use of sample and hold modules for input eliminates this problem since they hold the peak value of the input pulses. Thus the logarithmic ratio circuits see essentially d.c. inputs.

The trailing edge of the sample and hold pulse triggers monostable multivibrator A15. The output of A15 is about 20μsec wide. It acts as a delay one-shot, allowing sufficient time after the hold command for the logarithmic modules to reach their steady state output before data is actually taken. Its rising edge (since output is \bar{Q} this occurs 20μsec after hold command) triggers single-shot A16. A16 has an output pulse of approximately 2μsec and it controls the opening and closing of a CMOS switch (CD4016). Hence at this instant the switch closes for 2μsec, samples the value of the ratio and passes it into the pulse height analyzer. This switch is required to provide fast rise time pulses acceptable to the pulse height analyzer. The PHA will detect the value of the voltage pulse and store it in the appropriate channel. Single shot A16 also forms the input to a digital counter and this gives the total number of pulses counted. From this number and the time for which data is taken the average concentration of the particle stream can be determined.

The falling edge of the peak detecting pulse (A8) also triggers another monostable A14. The period of this is made longer than the total time required for a data point to be taken ($\sim 23\mu\text{sec}$). This pulse is fed into the input of nor gate A13, and once triggered, it clamps the output of the sample and hold command in the hold mode for a time equal to its pulse width.

When the pulse from A14 goes away, the measurement system is completely reset and is ready to accept new data.

Next, case b) is considered. This occurs when two particles arrive at the focal volume at slightly different instants so that there is a finite time during which both particles are scattering light from the laser beam. The result is an overlapping pulse like one shown in Figure 3-5b. The operation and timing of the circuit is as follows:

At first when the input exceeds the background discrimination level comparator A7 triggers as in the single pulse case. The circuit functions in exactly the same way, taking the ratio of the first peak and passing it to the pulse height analyzer. However, at the first dip, output of comparator A7 does not reset because the voltage level is still above the d.c. noise discrimination level. The comparator A8 will, however, reset to high because of its peak detecting characteristic. The output of nor gate A10 therefore goes high. Because the other input to A12 is held high by comparator A7, the output of A12 goes low. If by this time the preceding measuring cycle due to the first peak has terminated, output of monostable multivibrator A14 will be in low state. This allows the output of A13 to go high again. The sample and hold modules switch to the sample mode. When the peak of the second pulse is detected, the sample and hold modules change to hold mode and a new measuring cycle is initiated. It is seen that overlapping pulses which are not too close are recognized and counted by the circuit.

Finally, case c) is considered. This occurs when a chain of particles very close in space flows through the focal volume. The output will consist of a series of rippling pulses overriding on a certain d.c. level. Under such circumstances the ratio of the pulses are no longer accurate representation of their size. The circuit is designed to ignore most of these. Figure 3-5c shows the timing involved.

When the first pulse comes in the circuit operates in the same way as a) and b). The ratio of the first peak will be recorded. When the first dip comes output of comparator A8 will change state. However, because the ripples are close together, the output of monostable A14 is still high from the previous measuring cycle. This inhibits the sample command and clamps the sample and hold modules in the hold mode. When the next peak is detected the output of A8 goes low again. This high to low transition retriggers monostable A14 and keeps it in its high state. Thus no measurement cycle is initiated as long as the peaks are too close.

The point at which the circuit ceases to recognize overlapping pulses depends on the period of single shot A14. This can be adjusted to suit the flow rate of the particle stream through the focal volume. According to the concept outlined in Chapter II, this design should allow much higher concentrations to be detected without appreciable degradation in accuracy.

Chapter IV

EXPERIMENTAL METHODS, RESULTS AND ANALYSIS

This chapter describes the experiments performed on the system and discusses the results obtained. The response to artificially generated light pulses under various conditions were first analyzed. Then the system was tested and calibrated by monodisperse aerosols of known diameter and relatively low concentration. Finally, particle streams of high concentration were fed into the system to determine its concentration handling capacity.

4-1 Experiments Using Artificially Generated Pulses

In order to determine the response of the electronic system, an ideal source is required. This was implemented by an LED driven by a sinusoidal oscillator. The amplitude and pulse width of the output can be conveniently adjusted by changing the amplitude and frequency of the sinusoidal input. The optical module was not used and the LED was placed directly in front of the collection photomultiplier tubes. In this way the electronic circuit detected pulses whose ratio was a constant. Theoretically the pulse height analyzer should record a single channel distribution. The actual distribution obtained was about 10-15 channels wide and is shown in Figure 4-1. This broadening of the distribution could amount to a 5% uncertainty in particle sizes and is due to the following factors:

a) There is an inherent electronic spread in the circuit. This means that input pulses of a single ratio are recorded as pulses of slightly different ratios.

b) Optical spread due to the photomultipliers also causes broadening. This means that given a definite input intensity, the output current from each phototube would actually vary a little. This variation is due to differences in the photomultiplier characteristic and dark current.

The input pulse width was varied by adjusting the input sine wave frequency. It was found that no appreciable degradation of the output response occurred for a pulse width range of $\sim 800\mu\text{sec}$ to $30\mu\text{sec}$. The limit is set by the response of the peak-detector trigger circuit. If the pulse is too wide, it tends to rise very slowly and erratic peak triggering results. If the pulse is too narrow, the peak trigger tends to occur at a time when the input has long passed the peak value. A shift in the output distribution would result.

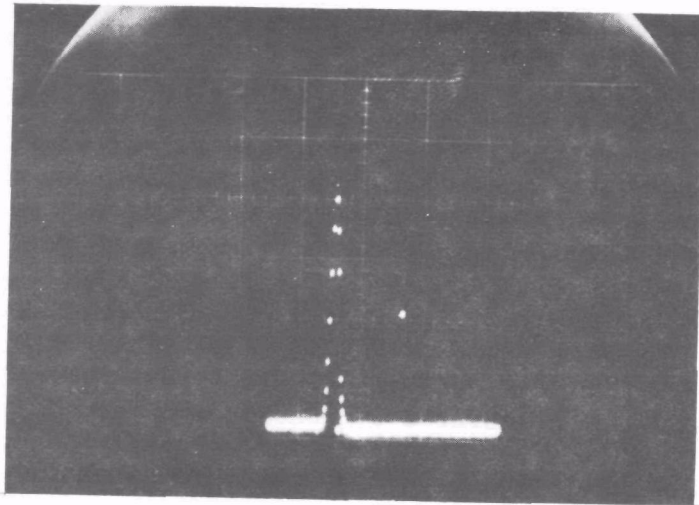


Figure 4-1. Typical distribution for artificial pulses of fixed ratio.

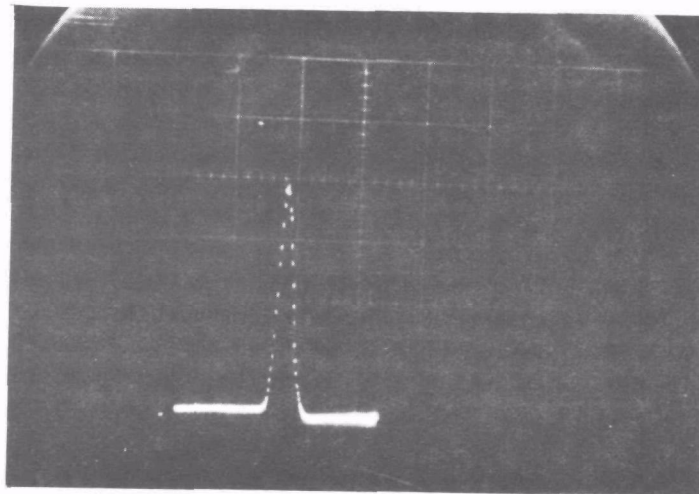


Figure 4-2. Distribution for fixed ratio pulses of very low amplitude.

This range of acceptable pulse widths limits the particle flow rate this instrument can measure correctly. For example, 100 μ m beam gives a pulse width of 100 μ sec for a flow rate of 100 cm/sec. However, by varying the time constant in the peak detector delay circuit, the system can be made to handle very slow or very fast flow rates.

The input intensity was varied by adjusting the amplitude. Theoretically no change in output ratio should occur. Experimentally the distribution obtained stayed practically constant for a large range of input pulse amplitudes unless the input amplitude is too low.

Signal to Noise Ratio Considerations

As the amplitude of the input pulses is reduced, noise inherent in the system becomes more and more prominent. The result is that the peak of the distribution stay constant but as a whole it became broader corresponding to a size uncertainty of a few percent. This is shown in Figure 4-2, where the input pulse amplitude is about 0.03V, corresponding to an input current of 3 μ A. This becomes important when measuring small particles since they scatter much less light. Big particles near the minimum in the forward lobe are also affected. There are two contributions to the noise in the system. One contribution is due to the dark current of the photomultipliers and the baseline noise of electronics. It is independent of the light source used. By using a laser source with big enough power, even very small particles can scatter enough light to make the noise unimportant. There is, however, another noise contribution which is due to stray light from the laser source that gets scattered off various parts of the optical collection module. The magnitude of this is proportional to the source laser power. Thus this signal to noise ratio cannot be improved by using a higher power laser. This part of the noise can be minimized by using antireflection coated lenses and better shielding of the collection system.

The response of the instrument to input pulses of different ratios was also investigated. A laser was chopped by a rotating plate with a small hole in it. The light that came through was then scattered off a translucent piece of plastic and collected by the two photomultiplier tubes. In this manner Gaussian shaped pulses very similar to those encountered in real particles were generated. The pulse width was about 150 μ sec. The ratio seen by the instrument was varied by inserting different neutral density filters in the path of either one of the phototubes. The maximum values of the input pulses were read from an oscilloscope and the corresponding distribution of the pulse height analyzer was recorded. Table 4-1 shows the results.

Table 4-1. Results of calibration using artificial sources.

Input on 10° PMT	Input on 5° PMT	Ratio 10°/5°	PHA Output (Channel No.)
2.2	1.4	1.56	40
2.2	1.95	1.12	70
2.2	3.2	0.69	140
2.2	3.6	0.60	180
1.6	3.4	0.47	220
1.6	3.9	0.41	260

A graph of input ratio (10°/5°) against output channel number is plotted in Figure 4-3. From this curve two points can be observed:

1) A larger input ratio results in a smaller channel number. This was intentionally done using a combination of a P-type module for the logarithmic ratio circuit and a N-type for the antilogarithmic module. If Figure 2-7 is referred to, one sees that as the particle size increases, the intensity ratio (10°/5°) decreases. Using this transfer characteristic, larger particles are placed to the right and smaller particles to the left in the output distribution.

2) The price paid for making the above adjustment is that the input output relationship is no longer linear. In fact if one refers to equations 3-1 and 3-3, it is seen that if the input to the antilog modules is $k \log \frac{i_1}{i_2}$, the output is not proportional to $\frac{i_1}{i_2}$ but rather $\frac{i_2}{i_1}$. The table below gives the values of 5°/10° against output channel number for the same set of data:

Table 4-2. Tabulation of I_5/I_{10} against output channel number.

I_{10}/I_5	I_5/I_{10}	Output Channel No.
1.56	0.64	40
1.12	0.89	70
0.69	1.45	140
0.60	1.68	180
0.47	2.13	220
0.41	2.44	260

A plot of I_5/I_{10} against output channel number is shown in Figure 4-4. It is linear, showing that the circuit performs as expected.

In order to check the ability of the instrument to detect two particles, an artificial source which generated two overlapping pulses was exposed to the photomultiplier tubes. The results are summarized in Figure 4-5. In Figure 4-5a the upper trace shows the input waveform as detected by the photomultipliers. The lower trace shows the output

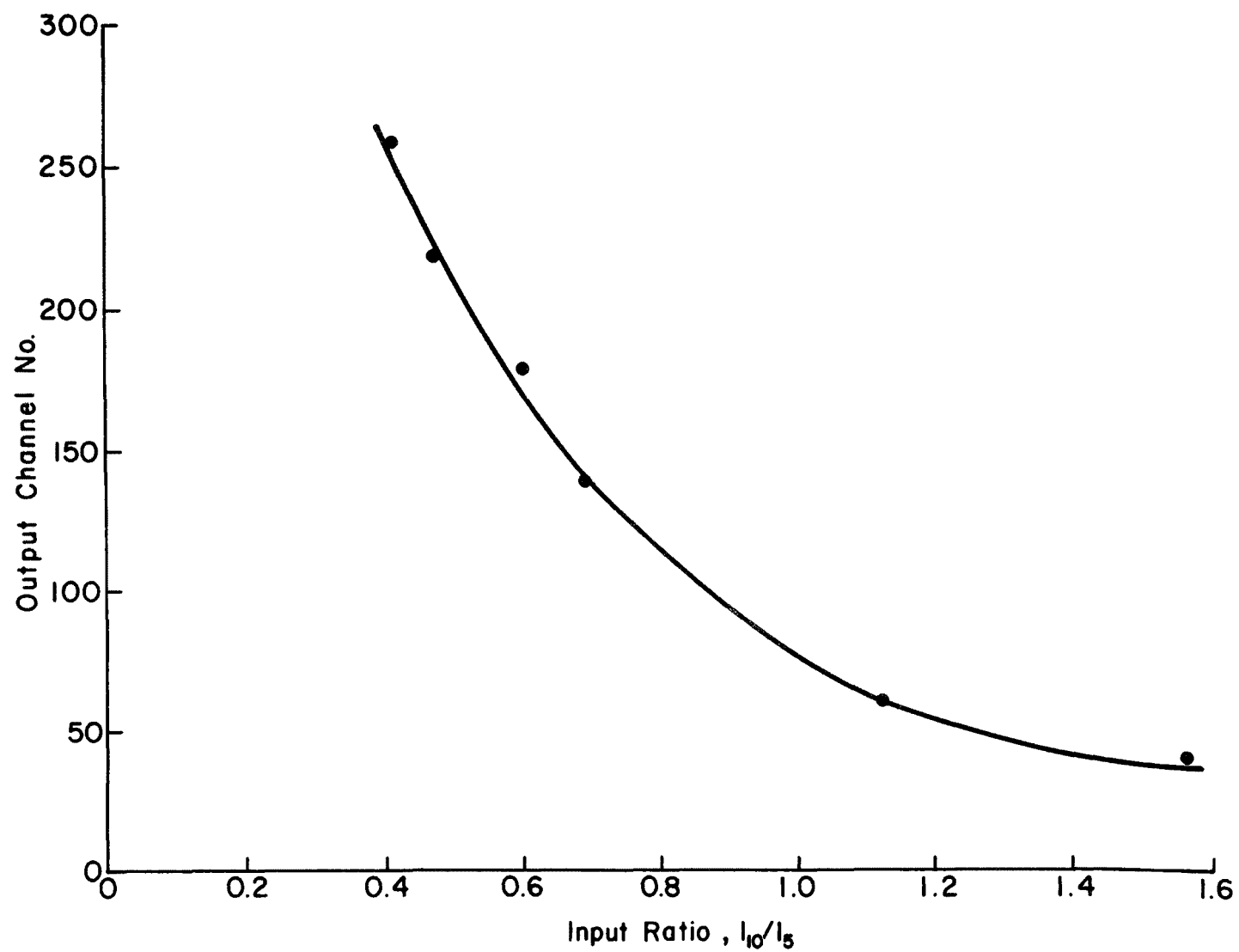


Figure 4-3. Output channel number plotted against input ratio (I_{10}/I_5).

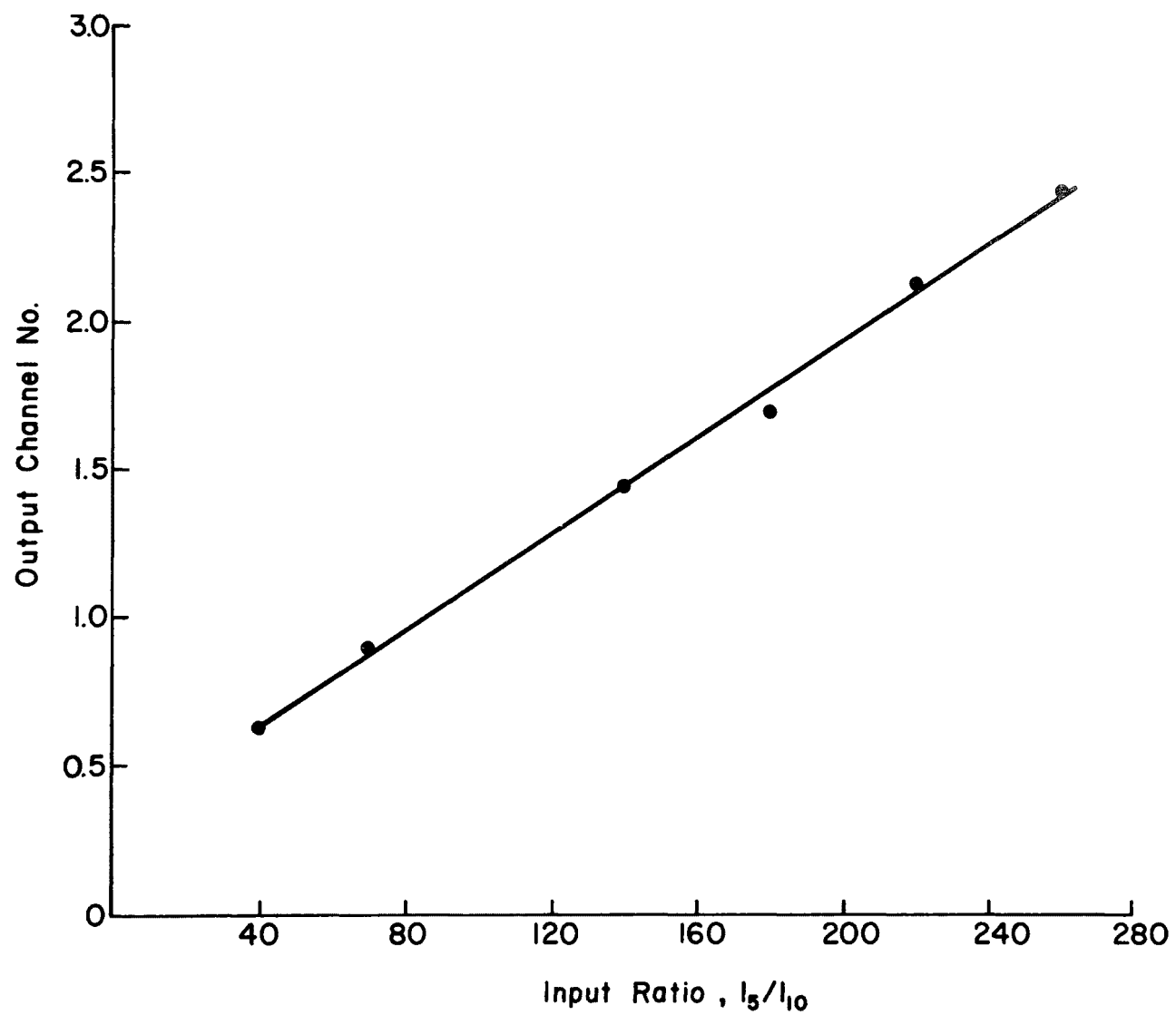
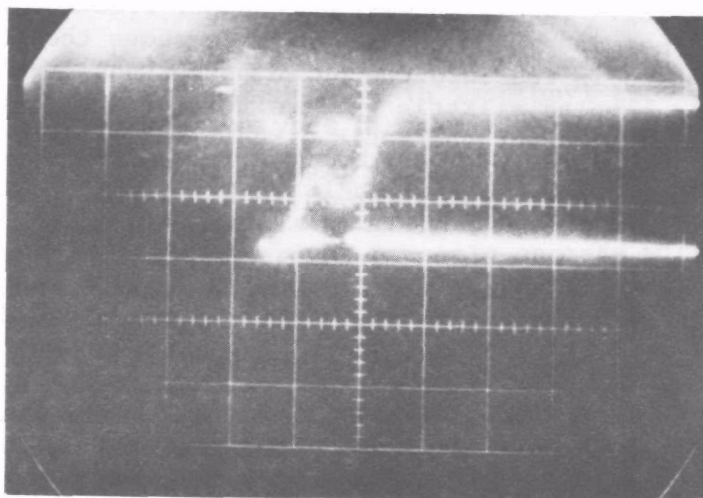
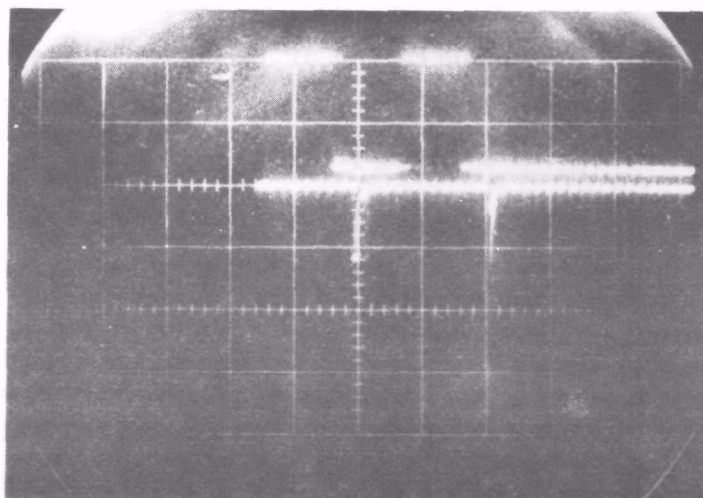


Figure 4-4. Output channel number plotted against input ratio (I_5/I_{10}).



(a)



(b)

Figure 4-5. Response of processing circuit to two overlapping pulses.

of gate A13 i.e., the sample and hold command. It is seen that the circuit successfully detects the peak values of the input and holds them for processing. In Figure 4-5b, the upper trace shows the same sample and hold command while the lower trace shows the output of the analog switch which is fed into the pulse height analyzer. One observes that the data is sampled a little while after the input hold command ($\sim 20\mu\text{sec}$) to allow time for the ratio circuit to settle down. The switch period is about $2\mu\text{sec}$. This demonstrates that the proposed circuitry can identify two pulses overlapping to about half the full width.

4-2 Tests Made on Real Particles

A) Calibration with Monodisperse Aerosols of Low Concentration

In order to calibrate this particle detecting system, a source providing uniform aerosols of known size is required. For this purpose the Berglund-Liu Monodisperse Aerosol Generator (Model 50A) was used.¹² In this particle generator, the desired aerosol is first dissolved in a volatile solvent in certain known concentrations. The resultant solution is then placed in a syringe. It is then pushed through a small orifice at a very steady rate by an infusion pump. The orifice is vibrating at a frequency which is controllable by an external sinusoidal oscillator. Under such conditions the solution stream is broken up into uniform droplets, one being generated for each cycle of disturbance. These droplets are then injected into a dry air flow which disperses them and dilutes them by a large amount. This large volume of air also allows the volatile solvent to evaporate, leaving the nonvolatile solute which then comes out as uniform particles. The diameter of the particles thus formed can be calculated as follows:

Let the volumetric concentration of the nonvolatile solute in the solvent be C.

The orifice vibration frequency be f Hz.

The liquid flow rate through the orifice be $Q\text{cm}^3/\text{sec}$.

Then, for each cycle of disturbance, the liquid drop generated would have a volume $\frac{Q}{f}\text{ cm}^3$.

After the volatile solvent has all evaporated, volume of the particle = $\frac{QC}{f}$.

Assuming the aerosol is a sphere, the diameter d is given by

$$d = \left[\frac{6QC}{\pi f} \right]^{1/3} \quad (4-1)$$

Since Q, C and f are all known quantities in an experiment, the diameter of the output aerosol need not be measured by another method (e.g., microscopy).

In the experiment methylene blue in isopropyl alcohol and water (50:50) and also Dioctyl Phthalate (DOP) in isopropyl alcohol were used as particle sources. These two types of particles have different refractive indices and can reveal the dependence of this ratio technique on refractive index. The particle diameter was varied by changing the frequency of the sinusoidal oscillator. The range thus obtained was not large since the particle generator can only operate within a limited range of frequencies. Using a 10 μ m orifice the operable frequency range was found experimentally to be 70KHz - 190KHz. To obtain a wider range of particle sizes, different concentrations were also used. The particles generated were allowed to flow through the focal volume and measurements taken. The particle diameter was calculated using equation 4-1. The table below shows the results of particle size with the channel number at the peak of the output distribution:

Table 4-3. Results of calibration using the Berglund-Liu generator.

(a) Dioctyl Phthalate (DOP).

Particle Diameter (μ m)	Channel No. at Peak of Distribution
3.23	270
2.82	160
2.57	130
2.04	96
1.62	105
1.28	78
1.01	66

(b) Methylene Blue.

Particle Diameter (μ m)	Channel No. at Peak of Distribution
3.37	290
2.67	170
2.12	122
1.68	95
1.47	90
1.33	80
1.16	75

If the concentration of the solution is too low, soluble impurities present in the solvent becomes a significant part. The diameter of the resultant particle can no longer be accurately determined by Equation 4-1. For this reason no quantitative data was taken for particles much smaller than 1 μm .

Figure 4-6 shows a plot of the particle size against output position on the pulse height analyzer for both DOP and methylene blue. Several characteristics of the two curves need to be discussed.

(1) First consider the curve for methylene blue particles. The theoretical curve (Figure 2-7) shows that the relationship of intensity ratio ($10^\circ/5^\circ$) to particle diameter should be fairly linear between 3 μm and 1.5 μm . The experimental curve is not linear but convex. This can be attributed to the fact that the circuit, instead of taking a ratio of $10^\circ/5^\circ$, actually takes the ratio $5^\circ/10^\circ$ as explained in section 4-1, where the same effect is observed when calibrating the instrument with known ratio pulses.

(2) If the intensity ratio method were perfect, the two curves shown in Figure 4-6 would overlap exactly i.e., particles of the same size would always have the same intensity ratio. This is obviously not true. To make it worse, the calibration curve for DOP shows a dip in the size range of 1.5-2.0 μm , making the instrument insensitive when sizing particles in that range. This dip is not observed for methylene blue. This discrepancy can be explained by the difference in refractive index of the two types of particles. Being transparent, DOP should have a refractive index which is almost real and its value is given to be 1.49. No specific information can be obtained concerning the refractive index of methylene blue. However, judging from its color, it should have a high imaginary component. Figure 4-7 shows theoretical curves of intensity ratio against particle sizes for various imaginary components of refractive index. This figure is reproduced after Kreikebaum and Shofner.¹⁰ The curves show that the intensity ratio is strictly decreasing with increasing particle size for large imaginary component of refractive index ($n_2 = 1.0$ and 0.2). These two curves are almost exactly the same. As the imaginary component becomes smaller, there is an increasing departure from the above characteristic and a flattening or dip can be observed for $n_2 = 0.05$, 0.01 and 0 . These curves are plotted for angles of 14° and 7° so that no quantitative comparison with the experimental results can be made. However, the ratio $10^\circ/5^\circ$ should follow the same general trend and one can qualitatively see that the experimental curves follow closely the theoretical predictions.

It would thus appear that the instrument gives much more accurate and consistent results when sizing highly absorbing particles. From the experimental curves, the maximum error incurred due to refractive index difference is around 20 percent.

(3) Another important criterion in evaluating the performance of this instrument is its resolution. Figure 4-8a and 4-8b show the actual

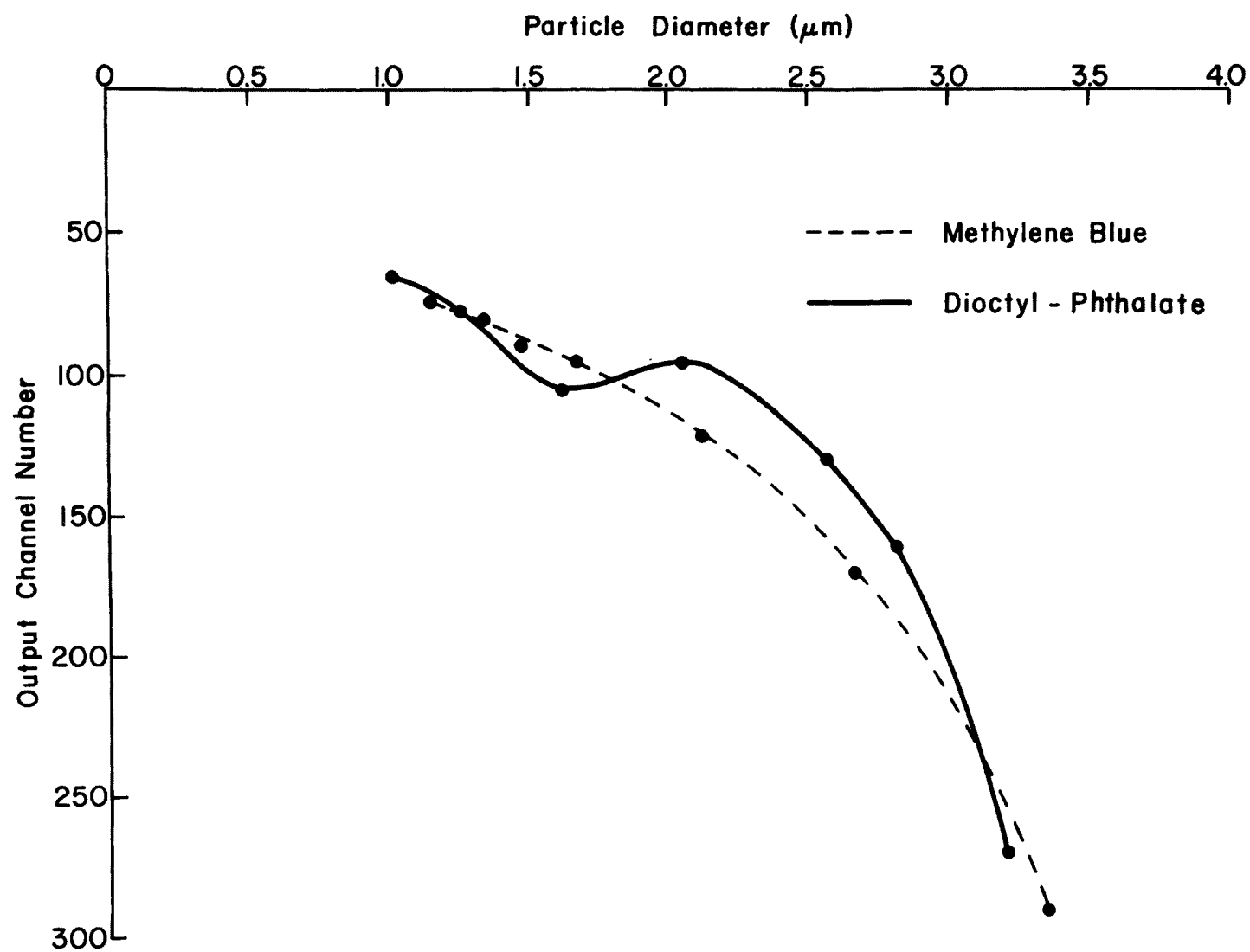


Figure 4-6. Calibration curves using methylene blue and DOP particles.

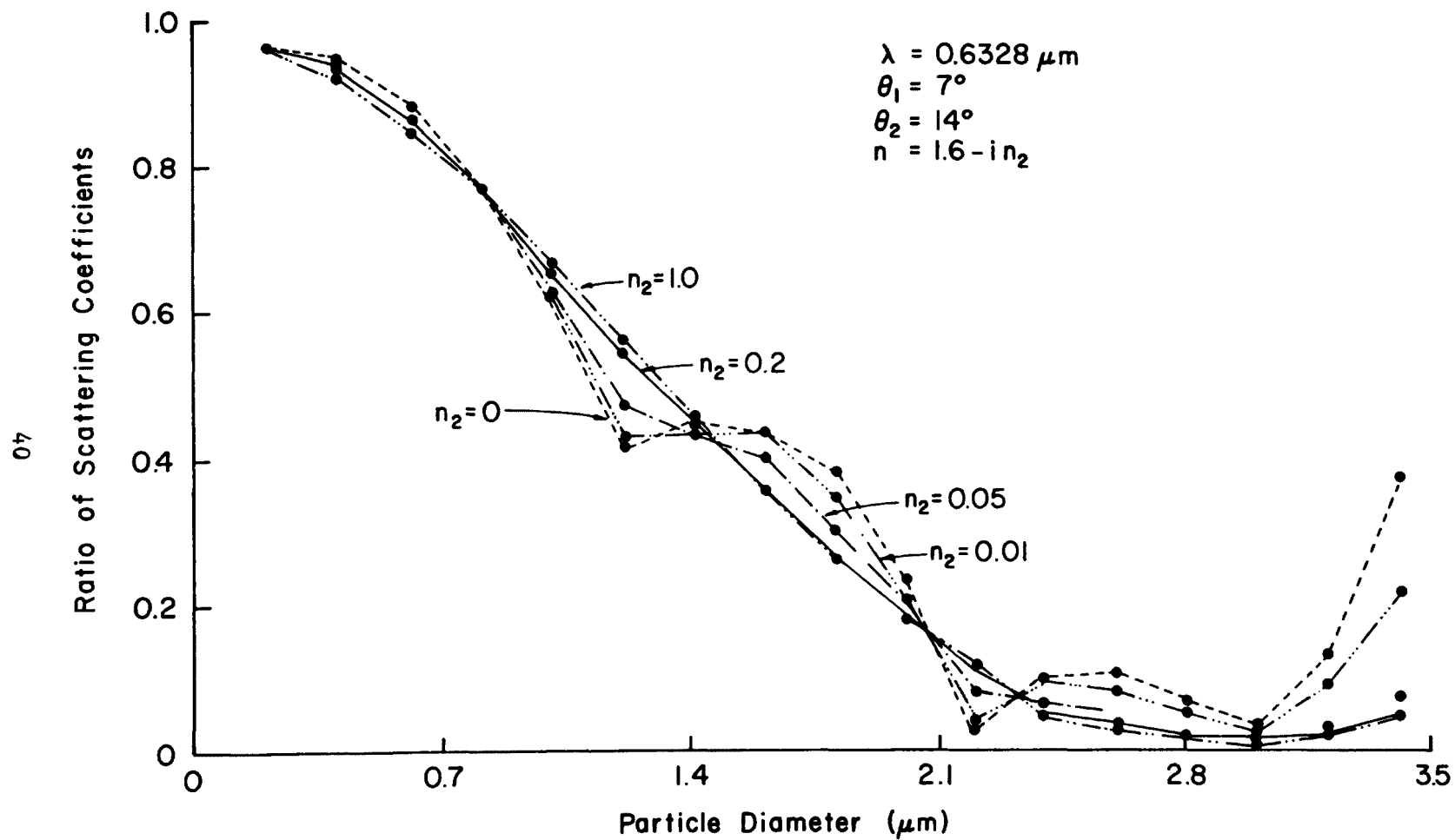


Figure 4-7. Intensity ratio against size for different refractive indices. Following Ref. 10.

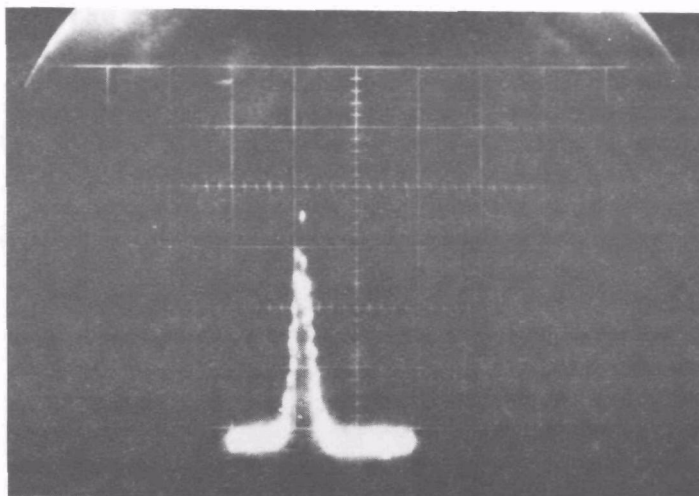


Figure 4-8a. Distribution for methylene blue particles of diameter 2.12 μm .

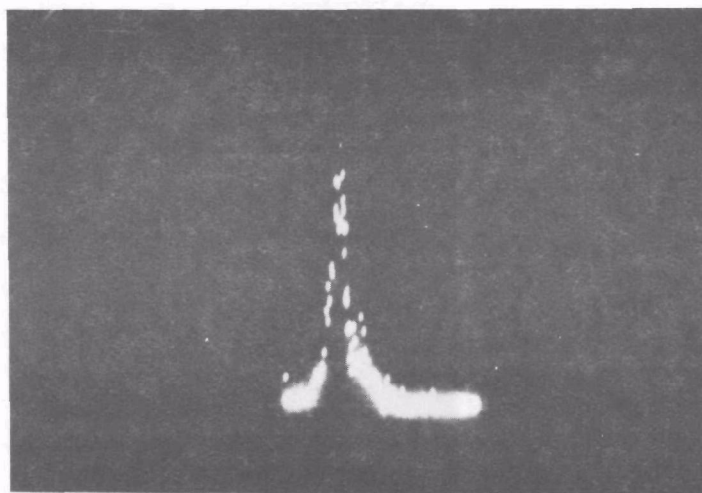


Figure 4-8b. Distribution for methylene blue particles of diameter 2.67 μm .

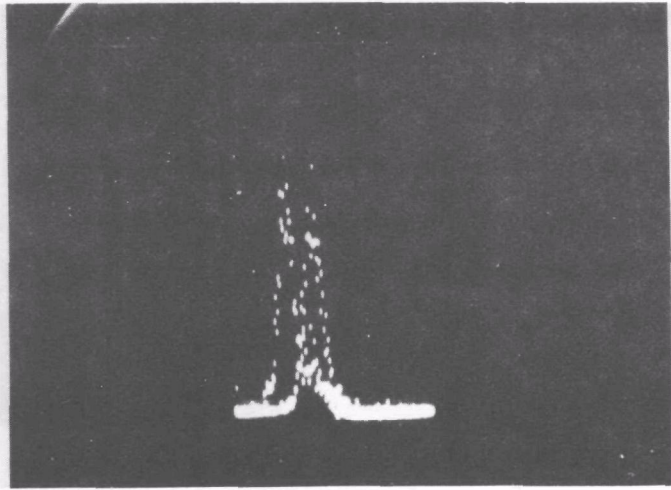


Figure 4-8c. The two above distributions superimposed on each other.



Figure 4-9. Distribution obtained using one photomultiplier.

distributions obtained on the pulse height analyzer for methylene blue particles of diameter 2.12 and 2.67 μm respectively. Figure 4-8c shows the two distributions superimposed on each other. The full width at half maximum of these distributions is approximately 20 percent of the maximum value. This is larger than that expected from a monodisperse aerosol. This broadening is not due to malfunctioning of the processing circuit. To prove this the following experiment was performed. The particle stream was allowed to pass through the focal volume. Instead of using two photomultiplier inputs, one photomultiplier was disconnected and the other photomultiplier output was connected to both inputs of the processing circuit. In this manner the circuit detected pulses of various amplitudes, but their ratio was constant. The distribution obtained is shown in Figure 4-9. It is only a few channels wide and it was discovered that variations in particle size did not change its position.

By using only one photomultiplier tube the variations due to different photomultipliers is eliminated and the width of the distribution is a measure of electronic spread only. The distribution shown in Figure 4-1 is broader than that in Figure 4-9. This indicates that phototube variations and dark current do contribute to some variations in ratio.

It was observed that the scattered light pulses were much bigger in amplitude than the background noise, so that the broadening cannot be explained on the basis of poor signal to noise ratio.

The spread can be accounted for if the following factors are considered:

(a) Imperfections of the particle generator--For ideal operation the particle generator should have a radioactive source in its drying column. This source ionizes the dilution air and the ionized air in turn neutralizes the charge on the aerosol particles. The above experiments were run without this source. The main effect is to cause deposition of the particles onto the walls of the drying column and the outlet, but there may be other undesirable effects resulting in a less uniform particle size. Another flaw is that the flow rate was not very uniform. This was determined by the steadiness of the infusion pump feed rate. During the experiment the clutch in the infusion pump was observed to slip occasionally. This would also give rise to non-uniformity in particle size. Therefore the standard deviation of the particles is expected to be higher than that claimed by the manufacturer (2-3 percent).

(b) Error in the optical collection system--The most important cause of broadening is the imperfection of the optical system. In order to give a constant ratio independent of position at which the particle passes through the beam, the relative response profile for the 5° and 10° collection should be exactly the same across the entire length of the focal volume. This was experimentally investigated. An intense, uniform jet of particles was blown through the laser beam. The diameter of the jet was much smaller than the length of the focal volume so that

relatively speaking, it could be considered as a point. The scattered pulses from the phototubes were fed directly into a pulse height analyzer. The average value of those pulses was determined by reading the peak of the resultant distribution. The jet was moved longitudinally across the length of the focal volume and the above data was taken at various points. From the data curves of the relative response of the 5° and 10° angles can be plotted. This is shown in Figure 4-10. One observes that the positions of the peaks are slightly different. This is due to spherical aberration which has not been fully compensated. The important thing is that even if the peak were exactly in the same position, the two profiles would still be different. The 10° profile has a larger value at the peak but it falls off much faster than the 5° profile. This means that a particle passing through the middle of the volume will give a different ratio from the same one passing through the ends. In the experiment a pair of parallel plates was used to direct the particle stream. Hence the effective focal volume was actually smaller, having a length of approximately 0.06 in (1.5 mm). With this length, the ratio spread is estimated from Figure 4-10 to be about 1:1.3. Obviously, this would result in a broader distribution than one expects.

The difference in the response profiles is due primarily to difference in geometry of the 5° and the 10° collection optics. A simplified theoretical analysis is given below.

Consider the case shown in Figure 4-11. A lens of focal length f is illuminated by an object placed at a distance u from its plane. The object has a finite height b which represents the finite diameter of the laser beam. Its intensity distribution is assumed to be Gaussian. An iris of diameter D limits the light and allows only light at a certain angle to pass through and get focused. The finite width of the slit is neglected. The light that comes through focuses at a distance v away from the lens. At this point a pinhole of diameter d collects the light. This represents the size of the optical fibre. This arrangement simulates the optical collection system used in this experiment. The pinhole is a two-dimensional circle, but a one-dimensional analysis with constant intensity shows approximately the same results.

From the basic lens equation

$$\frac{1}{u} + \frac{1}{v} = 1/f$$

$$v = \frac{fu}{u-f} .$$

Taking the differential on both sides

$$dv = \frac{-f^2}{(u-f)^2} du \quad (4-2)$$

The magnification of the image is given by

$$m = \frac{v}{u} \quad (4-3)$$

If the object is at exactly u from the lens plane, the intensity distribution on the image plane will be Gaussian centered on the axis as shown in Figure 4-11b.

If the object is at a distance $u + du$ from the lens, the image will be focused closer to the lens. The light will diverge out after they focus at the point $v + dv$. At the position of the pinhole the intensity distribution will be two Gaussian shapes, each displaced from the axis by an amount δ and having peak intensity half the original value.

The same result is obtained if the object is at a distance $u - du$ from the lens. This time the image is formed further away from the lens, and the pinhole sees the converging beam. The displacements are assumed to be small so that the quantity δ is the same for same change in positive and negative directions.

The value of δ is related to the geometry of the arrangement. Referring to Figure 4-11c and assuming small displacements, similar triangles give

$$\begin{aligned} \frac{\delta}{D/2} &= \frac{dv}{dv+v} \\ &= \frac{dv}{v} . \end{aligned}$$

$$\text{Hence } \delta = \frac{D}{2v} dv \quad (4-4)$$

At any position of the object the total power falling on the collection pinhole is given by

$$\int_{-1}^{+1} I_o e^{-[(x-\delta)/a']^2} dx + \int_{-1}^{+1} I_o e^{-[(x+\delta)/a']^2} dx \quad (4-5)$$

where I_o = peak intensity and $1 = d/2$.

a' is related to the input Gaussian constant a by $a' = ma$. Consider the term

$$\int_{-1}^{+1} e^{-[(x+\delta)/a']^2} dx$$

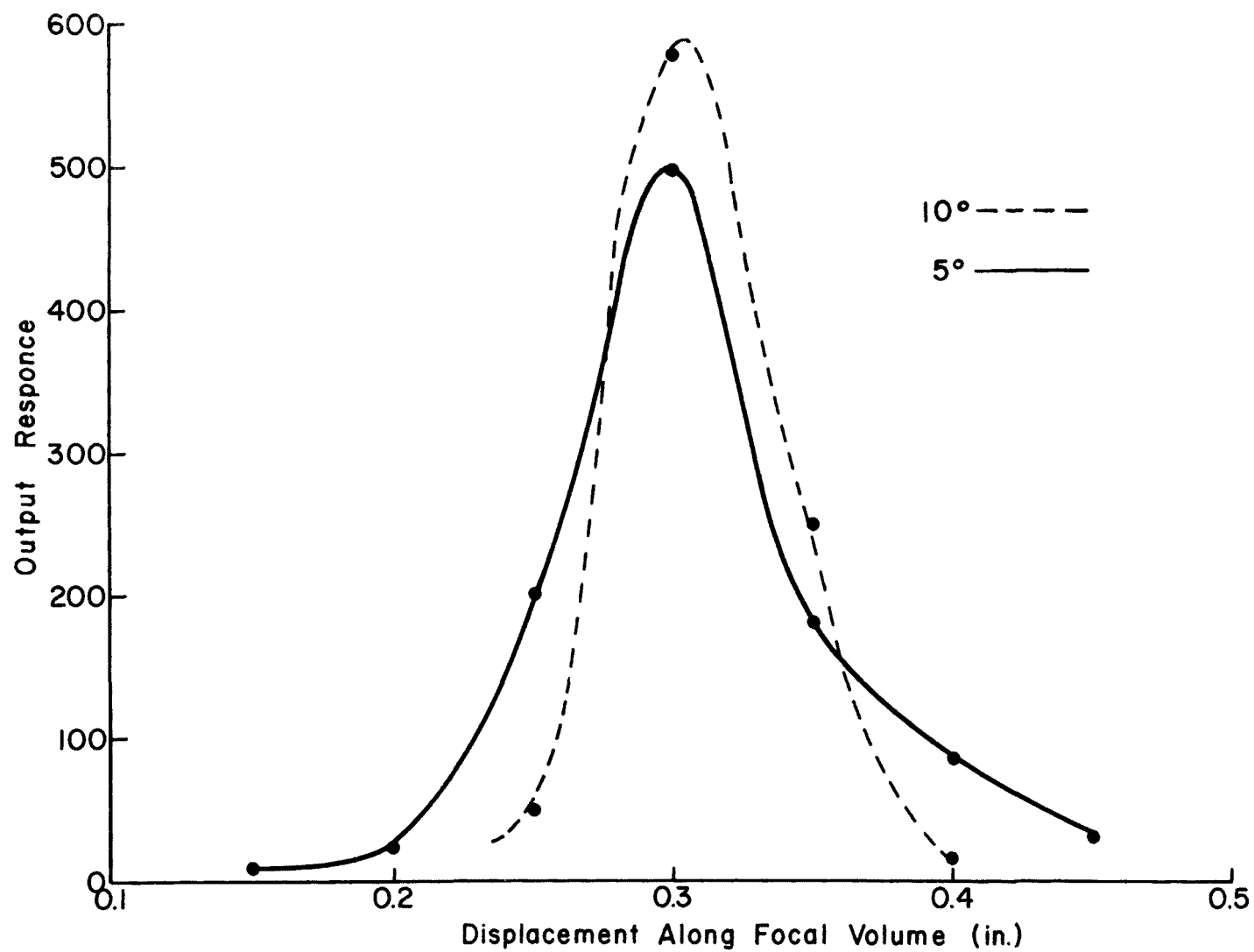
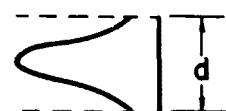
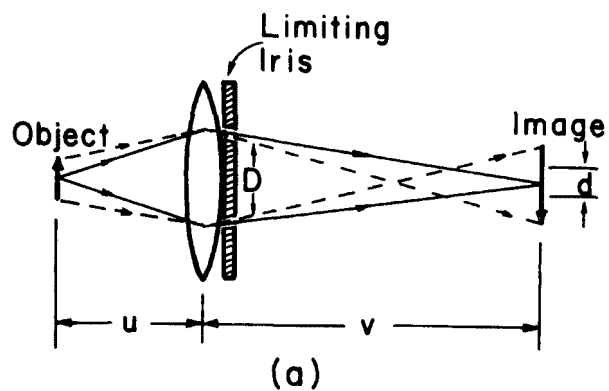
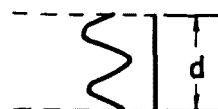


Figure 4-10. Relative response profiles for the 5° and 10° collection systems.

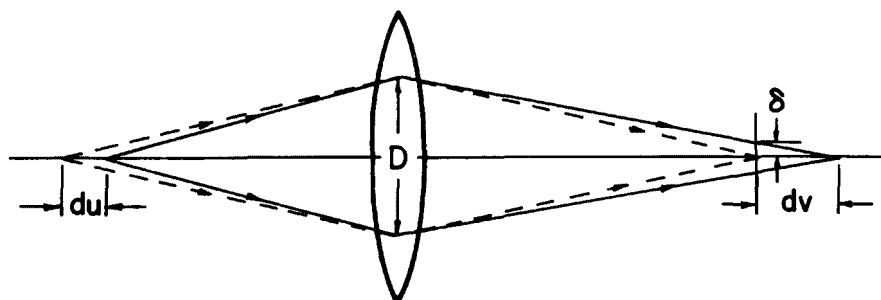


Exactly in Focus



Slightly Out of Focus

(b)



(c)

Figure 4-11. Simplified optical collection system for theoretical analysis.

Putting $y = -x$, the integral becomes

$$= \int_{-1}^{+1} e^{-[(y-\delta)/a']^2} dy$$

Hence the two integrals in equation 4-5 are equal. Total power

$$= 2I_0 \int_{-1}^{+1} e^{-[(x-\delta)/a']^2} dx \quad (4-6)$$

If the diameter of the beam is taken as the $\frac{1}{e}$ points, the quantity a is given by

$$\frac{\frac{b^2}{4}}{a^2} = 2$$

$$a^2 = \frac{b^2}{8}$$

$$\text{Hence } a'^2 = \left(\frac{v}{u}\right)^2 \frac{b^2}{8} . \quad (4-7)$$

The total power intercepted for various values of du can be numerically calculated. The only difference between the 5° and 10° arrangement is that the diameter of the iris (D) is different. Table 4-4 shows the theoretical results for the following typical values of u , v , f , D and d .

$$f = 4 \text{ cm}$$

$$u = 6 \text{ cm}$$

$$v = 12 \text{ cm}$$

$$d = 0.12 \text{ cm}$$

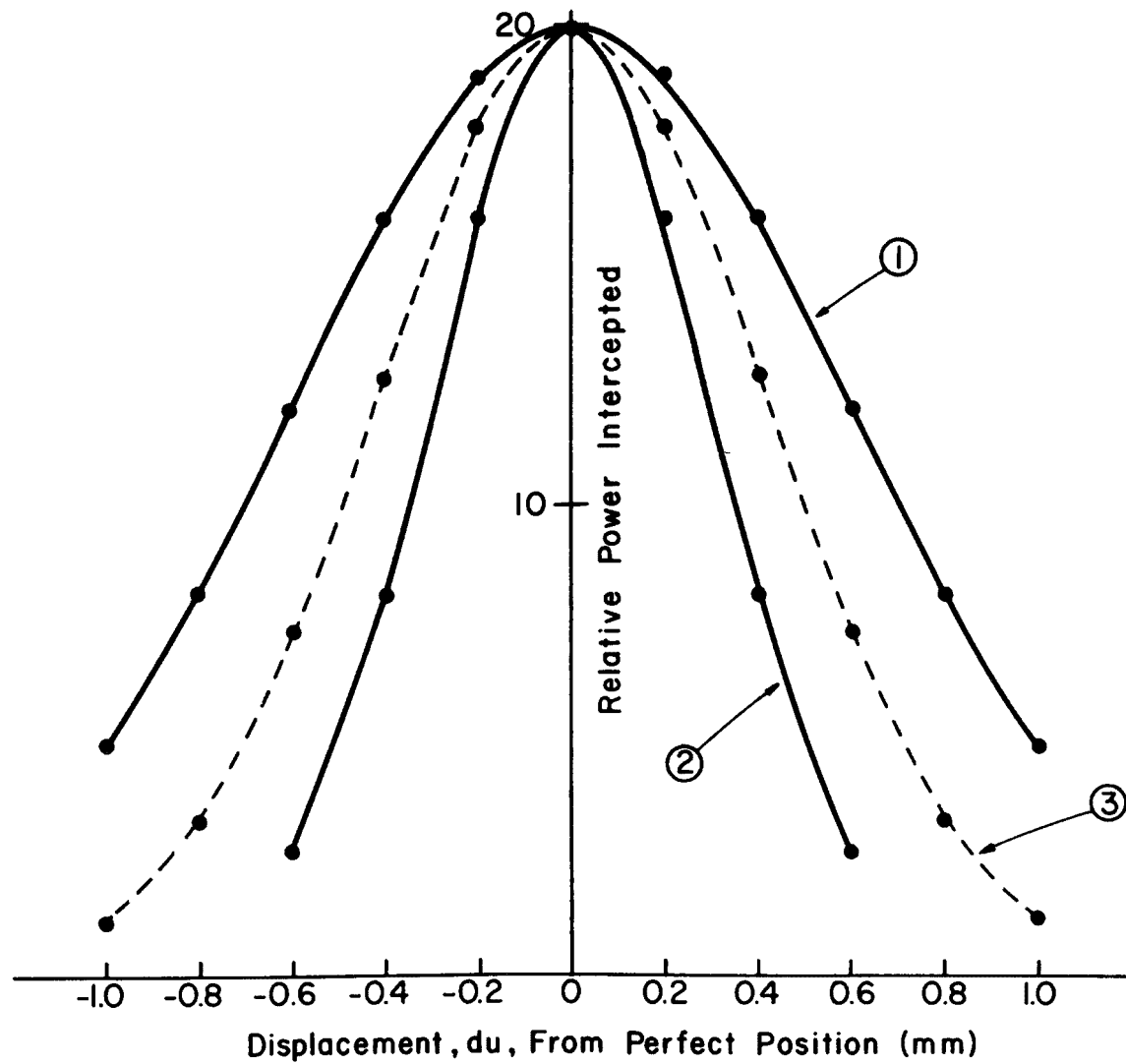


Figure 4-12. Theoretical plots of relative power intercepted against displacement for different values of iris diameter.

Table 4-4. Theoretical values of intercepted power against position.

du (mm)	Intercepted Power (unnormalized)		
	D=3cm, b=0.12cm	D=6cm, b=0.12cm	D=3cm, b=0.085cm
-1.0	4.907		1.194
-0.8	8.143		3.296
-0.6	12.072	2.641	7.260
-0.4	15.905	8.143	12.755
-0.2	18.907	15.985	17.878
0	19.976	19.976	19.908
0.2	18.907	15.985	17.878
0.4	15.985	8.143	12.755
0.6	12.072	2.641	7.260
0.8	8.143		3.296
1.0	4.907		1.194

Curves of intercepted power against du are plotted for the three cases in Figure 4-12. The first and second correspond to the same beam diameter but two different angles, while the third one corresponds to a smaller beam diameter.

From the curves 1 and 2 it is seen that a difference in collection angle results in a difference in response profile. The one with larger angle falls off much faster. These two curves have very similar shape to the experimental ones shown in Figure 4-10.

Case three is a case with a beam diameter $\sqrt{2}/2$ times smaller. When compared with case one (since they have the same collection angle), it has a smaller spread. This indicates that the diameter of the beam has a significant effect on the length of the focal volume.

The above theoretical analysis shows that the difference in response profile is inherent in the optical system. If the two angles are to respond in exactly the same way, the quantity δ must be the same for a change in object distance u. From equation 4-4, since D is not the same for the two angles, it requires that dv be different to compensate for this. With these equations and the required conditions, it is possible to design an optical collection system with exactly the same profile for both angles.

The above discussion suggests that the resolution ambiguity due mainly to the poor collection system is 10 percent or $\pm 0.05 \mu\text{m}$ at $1.0 \mu\text{m}$. This represents a major problem for the current optical module.

(4) Range of Sizing--One theoretical limit for the intensity ratio technique is that the curve of intensity ratio against size is flat at small sizes. A practical limitation is that the scattered signal becomes small and signal to noise ratio degrades as size is decreased. For a $10^\circ/5^\circ$ and laser wavelength of $0.6\text{ }\mu\text{m}$, this theoretical limit is around $0.3\text{ }\mu\text{m}$. The laser power of 5 mw is sufficient to give a reasonable signal. However, because of the inherent optical spread the size resolution goes down as particle size is decreased. No quantitative data has been taken, but the lower limit is estimated to be around $0.6\text{ }\mu\text{m}$.

For bigger particles the limit is set by the point at which the scattered intensity goes out of the forward lobe. The maximum size that can be handled is around $3.5\text{ }\mu\text{m}$ for $10^\circ/5^\circ$. One disadvantage of the ratio technique is that the relationship of particle size to intensity ratio is not single valued. Error due to this becomes large when sizing a distribution of particles which has a lot of big ones. Methods such as an upper intensity cutoff (suggested by Gravatt)¹³ or the use of a third angle (suggested by Hirleman and Witting)¹⁴ may be used to reduce sizing error.

B) Tests on Particles of High Concentration

The Berglund-Liu particle generator can only provide particles of relatively low concentration (~ a few hundred/cc). The scattered light pulses observed on an oscilloscope were widely separated. It was not possible to get quantitative data concerning the maximum concentration that can be handled by the instrument. A source which generates a particle stream of high concentration with a time invariant particle size distribution is required. It would be advantageous to be able to vary the particle stream concentration. A DOP smoke generator was used.¹⁵ This generator is a collision type atomizer. Basically the operation of this atomizer is as follows: A jet of compressed air is blasted into the liquid DOP solution. The air stream interacts with the liquid, generating small disturbances on the liquid surface. The turbulent jet drags out fine ligaments of liquid from the bulk liquid stream. Finally, these ligaments break up into small droplets because of surface tension effects.

There is no specific information on the size of the particles generated this way. However, they are estimated to be around the range of $1\text{--}5\text{ }\mu\text{m}$ and are quite uniform. The concentration that can be achieved is very large.

The experimental setup consisted of applying a jet of compressed air to the atomizer. The output aerosol was then directed to a T, where it was allowed to mix with a large volume flow of dry air. By adjusting the flow rate of the dilution air, the concentration of DOP particles could be controlled. The diluted particle flow was then coupled to a pair of parallel plates which directed the particle stream to the focal volume, limiting the effective focal volume to be about

1.5 mm. Along one side of the coupling there was an adjustable bypass. This was used to divert a part of the particle stream, regulating the flow rate through the focal volume. This prevented the stream from flowing too fast when the dilution was high.

The experiment was started with a very large flow of dilution air so that the concentration was low. The distribution obtained was recorded for comparison. Then the dilution air was reduced step by step. The output distribution was again recorded and compared with the one obtained previously. The amount of flow diverted from the main stream was accordingly varied to keep the output flow rate quite constant.

When the particle concentration is large, the count rate on the digital counter does not truly represent the total number of particles passing through the focal volume per unit time since the more closely overlapped ones are neglected. The output of comparator A8 is a convenient point to monitor. The reason is that it triggers on every peak and would count all the particles.

The count rate at output of A8 and the actual rate of data acquisition (at the digital counter) was recorded for each value of concentration. The width of the pulses scattered from the focal volume was monitored on the oscilloscope. During the entire process the pressure of compressed air applied to the atomizer was kept constant.

It was found that the output distribution remained fairly constant as the concentration was increased. At an input count rate of 21KHz, the output distribution was just a little broader than the dilute case, and the peak of the distribution was in the same position. Even at 32KHz input rate the peak stayed in approximately the same place although the distribution was considerably broader. Further increase in concentration resulted in an almost steady d.c. offset in the photomultiplier outputs and the output count rate dropped drastically. The count rates for higher concentrations are given in the table below:

Diameter of beam = 0.2 mm

Effective length of focal volume = 1.5 mm

Output pulse width = 100 μ sec

Period on monostable A14 = 60 μ sec.

Table 4-5. Experimental results for DOP smoke.

Input count rate f (at A8)	Output count rate f' (at A16)
9.5KHz	7.0KHz
12.0KHz	7.7KHz
21.0KHz	8.5KHz
32.0KHz	8.0KHz

The concentration of the particle stream at different input count rates can be calculated as follows:

The velocity of the particles through the laser beam

$$= \frac{\text{Diameter of beam}}{\text{transit time}}$$

$$= 200 \text{ cm/sec.}$$

If the laser beam has a diameter b and effective length of focal volume is l , in one second the particle stream would sweep out a volume lbv .

$$\text{Substitute in actual numbers, volume swept out} = 0.6 \text{ cm}^3.$$

If the input count rate is f/sec , the average concentration of the particles will be $\frac{f}{0.6}/\text{cm}^3$.

The focal volume seen by the particle stream is calculated assuming a circular laser beam and hence a cylindrical volume.

$$\begin{aligned} \text{This is given by } \pi \frac{(0.02)^2}{4} \times 0.15 \text{ cm}^3 \\ = 4.7 \times 10^{-5} \text{ cm}^3. \end{aligned}$$

The average number of particles present in the focal volume at any instant (\bar{N}) is equal to average concentration multiplied by the focal volume.

Corresponding to a certain \bar{N} , there is a certain value of probability of 1,2--etc. particles in the focal volume according to the Poission distribution outlined in Chapter II. If the instrument is handling single particles only, then the fraction of particles that gets counted would be given approximately by

$$\begin{aligned} \frac{P(1)}{P(1) + P(2) + P(3) + \dots + P(n)} \\ = \frac{P(1)}{1 - P(0)}. \end{aligned}$$

The approximate fraction of particles counted if both single and double pulses are handled is

$$\frac{P(1) + P(2)}{1 - P(0)}.$$

Using the above formulae the theoretical values of $\frac{P(1)}{1 - P(0)}$ and $\frac{P(1) + P(2)}{1 - P(0)}$ can be calculated for the different concentrations. This

can be compared with the experimental count rates. The following table summarizes the results:

Table 4-6. Comparison of Theoretical and Experimental Count Rates.

f (KHz)	f'(KHz)	Average concentration (particles/cm ³)	\bar{N}	f'/f	$\frac{P(1)}{1-P(0)}$	$\frac{P(1) + P(2)}{1-P(0)}$
9.5	7	1.58×10^4	0.74	0.74	0.66	0.88
12	7.7	2×10^4	0.94	0.66	0.61	0.91
21	8.5	3.5×10^4	1.65	0.40	0.39	0.70
32	8	5.3×10^4	2.51	0.25	0.22	0.50

The above table shows that the experimental fractional count rate is always slightly bigger than $\frac{P(1)}{1-P(0)}$ but smaller than $\frac{P(1) + P(2)}{1-P(0)}$. This shows that the instrument is counting single pulses and also double ones that are not closely spaced.

Figure 4-13 shows a typical distribution obtained on the pulse height analyzer. From its position the size of the particles would be from 1.5-2.5 μ m. There is no accurate way to check the size by another method. A rough estimate was made by collecting some of the particles on a slide and looking at them under a microscope. They appear to be larger than the instrument reading. This is probably due to coagulation and flattening of the oil droplets on the slide.

In summary, the above experimental results indicate that the present instrument can size particles with reasonable accuracy up to $\bar{N} = 1.65$. If larger errors can be tolerated, it can operate up to $\bar{N} = 2.5$. Even if $\bar{N} = 1.65$, it means an improvement of a factor of 8 in concentration handling capability over the single particle counter.

The actual concentration that can be handled is only $5.3 \times 10^4/\text{cm}^3$. This is because the focal volume in this case is quite large ($4.7 \times 10^{-5} \text{cm}^3$). With better laser focusing and better optical collection, the focal volume can be reduced to around 10^{-7}cm^3 . With such volume concentrations as high as $2 \times 10^7/\text{cm}^3$ can be sized by this instrument.

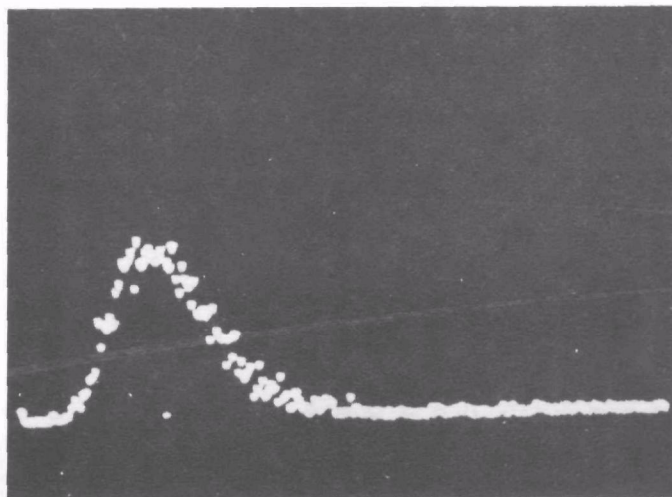


Figure 4-13. Typical distribution for DOP smoke of high concentration.

Chapter V

SUMMARY AND FUTURE WORK

A light scattering instrument for measuring size distributions of dense particulate systems in real time has been developed. It is based on the concept of allowing more than one particle in the focal volume at the same time and selectively processing the scattered light pulses by proper electronic circuitry. This selection process is entirely random as far as particle size is concerned. Hence the size distribution is not altered.

This instrument was calibrated with methylene blue and DOP particles. The calibration reveals that an error of ~20 percent is incurred due to difference in refractive index. If the index of refraction of the particle cloud is known, the intensity ratio technique may not be the most accurate one for sizing. However, for particles with unknown refractive indices, this method is superior compared to other optical methods.

The theoretical limits for the size range is from 0.3 to 3.5 μ m using the present configuration. Experimentally, the range was found to be 0.6 to 3.5 μ m due to various imperfections. As pointed out in Chapter I, this range of sizes is of high concern in air pollution studies.

The resolution of the instrument was found to be not as good as expected. This was due to imperfect design of the optical collection system resulting in different response profiles for the 5° and 10° detectors. With a better designed collection system, it is possible to improve the resolution by a factor of two or three.

The instrument was tested with DOP smoke and its performance was consistent with predictions by probability theory. Concentration up to $\bar{N} = 2.5$ has been tested and the results were satisfactory. This represents an improvement of an order of magnitude over previous optical sizing devices using an intensity-ratio technique. It was shown that, with tighter focusing, say, a focal volume of 2×10^{-7} cm³ used by previous investigators, concentrations as high as 10^7 particles/cm³ can be sized in real-time by our technique.

The ultimate goal of this work is to develop a practical, rugged real-time particle size monitoring system for source evaluations. The validity of the concepts outlined in Chapter II have already been

demonstrated by the experimental results. Hence, future work would involve the refinement of the present system, especially the optical module, to improve both the actual concentration handling capability and resolution of this instrument. Since the range of particle size is limited, efforts should also be directed towards increasing the sizable range. In this connection, a shorter-wavelength laser with a different choice of collection angles might be used and the possibility of using back scattering should be investigated.

REFERENCES

1. Belden, L. H., and Penney, D. M., "Optical Measurement of Particle Size Distribution and Concentration." General Electric technical information series (February 1972).
2. Apichatanon, O., "Measuring Aerosol Size Distributions," M. S. Thesis, Colorado State University (1974).
3. Liu, Y. H., Berglund, R. N., and Agarwal, J. K., "Experimental Studies of Optical Particle Counters." Atmospheric Environment Vol. 8 (1974).
4. Hodkinson, J. R., "Particle Sizing by Means of the Forward Scattering Lobe." Applied Optics 5:5 (May 1966).
5. Hodkinson, J. R., Electromagnetic-Scattering, edited by Milton Kerker (Pergamon Press, London, 1963).
6. Mie, G., Ann. Physik 35, 377 (1908).
7. Van De Hulst, H. S., Light Scattering by Small Particles. (Wiley and Sons, New York, 1957).
8. Born, M., and Wolf, E., Principles of Optics. (McGraw-Hill, New York, 1941).
9. Denman, H. D., Heller, W., and Pangonis, W. J., Angular Scattering Functions for Spheres. (Wayne State University Press, 1966).
10. Kreikebaum, G., and Shofner, F. M., "Design Considerations and Field Performance for an in situ, Continuous Fine Particulate Monitor Based on Ratio-Type Light Scattering." Presented at the International Conference of Environmental Sensing and Assessment (1975).
11. She, C. Y., and Chan, P. W., "Real Time Particle Sizing: Increasing the capability of the Instantaneous Scattered Intensity Ratio Technique." Applied Optics, Vol. 14. p. 1767 (August 1975).
12. Berglund-Liu Monodisperse Aerosol Generator Operation Manual.
13. Gravatt, C. C., "Light Scattering Methods for the Characterization of Particulate Matter in Real Time."
14. Hirleman, E. D., Jr., and Witting, S. L. K., "In Situ Optical Measurement of Automobile Exhaust Gas Particulate Size Distributions: Regular Fuel and Methanol Mixtures." Presented at the Symposium on Combustion, Boston (1976).
15. Yang, B. T., and Meroney, R. N., "On Diffusion from an Instantaneous Point Source in a Neutrally Stratified Turbulent Boundary Layer with a Laser Light Scattering Probe." Technical Report No. 20, Office of Naval Research.

TECHNICAL REPORT DATA
(Please read Instructions on the reverse before completing)

1. REPORT NO. EPA-600/2-77-022		2.	3. RECIPIENT'S ACCESSION NO.	
4. TITLE AND SUBTITLE A Real-Time Measuring Device for Dense Particulate Systems			5. REPORT DATE January 1977	
7. AUTHOR(S) P.W. Chan, C.Y. She, C.W. Ho, and A. Tueton			6. PERFORMING ORGANIZATION CODE	
9. PERFORMING ORGANIZATION NAME AND ADDRESS Colorado State University Fort Collins, Colorado 80523			8. PERFORMING ORGANIZATION REPORT NO.	
12. SPONSORING AGENCY NAME AND ADDRESS EPA, Office of Research and Development Industrial Environmental Research Laboratory Research Triangle Park, NC 27711			10. PROGRAM ELEMENT NO. LAB012; ROAP 21ADL-018	
			11. CONTRACT/GRANT NO. Grant R803532-01-0	
15. SUPPLEMENTARY NOTES IERL-RTP Project Officer for this report is W. B. Kuykendal, 919/549-8411 Ext 2557, Mail Drop 62.			13. TYPE OF REPORT AND PERIOD COVERED Final; 6/75-8/76	
16. ABSTRACT The report describes the design and performance of an instrument, based on the concept of instantaneous intensity ratio, for measuring particle size distributions of dense particulate matter. The method involves simultaneously measuring the intensity of light scattered by a particle at two small angles, and then taking their ratio. The ratio depends on particle size, but has minimal dependence on refractive index. By using a pulse height analyzer as the display device, particle size distribution changes can be detected rapidly. Thus in situ, real-time monitoring of size distributions can be achieved. The instrument allows more than one particle in the focal volume at any instant and selects the scattered light pulses randomly for processing, enabling dense particulate matter to be sized accurately. The concept is discussed. The instrument's detailed design features are presented. Calibration has been performed using monodisperse aerosols of accurately known diameter. The effect of refractive index is investigated, and the performance and limitations of the instrument are discussed. It is shown that, by incorporating the concept of random selection of input pulses, the concentration handling capacity is improved by an order of magnitude.			14. SPONSORING AGENCY CODE EPA-ORD	
17. KEY WORDS AND DOCUMENT ANALYSIS				
a. DESCRIPTORS		b. IDENTIFIERS/OPEN ENDED TERMS		c. COSATI Field/Group
Air Pollution Aerosols Dust Measurement Refractivity		Air Pollution Control Stationary Sources Particulate Instantaneous Intensity Ratio Real Time		13B 07D 11G 14B 20F
18. DISTRIBUTION STATEMENT Unlimited		19. SECURITY CLASS (This Report) Unclassified		21. NO. OF PAGES 66
		20. SECURITY CLASS (This page) Unclassified		22. PRICE